(Un)intended Consequence of Extreme Heatwaves on Air Pollution and Its Social Cost: Evidence from the Power Sector in China*

Pin Sun[a], Yu'an Wang[a], Yang Wang[b], Wei Dai[a], Qingchen Chao[b],

Bowei Guo[a], Chenpeng Wang[b]

October 7, 2025

Abstract

Extreme heatwaves undermine the efficiency of fossil-fuel power generation, amplifying air pollution and health risks. Using plant-level operational and high-resolution weather data from China, we estimate that heatwaves raise $PM_{2.5}$ emission intensity by 21.4% on average, with coal-fired units experiencing an additional 12.3% increase relative to gas-fired plants. Similar patterns hold for other combustion-related pollutants. We estimate that heatwave-induced pollution imposes an annual social cost of USD 4.21 billion in China, which could be reduced by USD 1.42 billion under a complete shift from coal to gas. Looking ahead, under the high-emissions SSP5-8.5 scenario, which implies about 4.4° of warming by 2100, annual costs in China could rise to USD 20.41 billion. The impacts are highly uneven across provinces, with coal-dependent and industrial coastal regions disproportionately affected. Globally, such efficiency losses impose USD 76.21 billion in annual damages, with India and China together bearing most of the burden. But coal-to-gas substitution strategy could substantially mitigate these losses. Our findings highlight how climate extremes can amplify air pollution and health damages through overlooked energy-sector channels, underscoring the broader societal costs of continued fossil-fuel dependence in a continued warming world.

Keywords: Extreme Heatwaves; Power Plant Efficiency; Air Pollution; Social Cost

1 Introduction

Extreme heat is intensifying worldwide under human-induced climate change. Between May 2024 and May 2025, the hottest 12-month period ever recorded, around 4 billion people ex-

*Affiliations: [a]School of Applied Economics, Renmin University of China, Beijing 100872, China; [b]China Meteorological Administration Key Laboratory for Climate Prediction Studies, National Climate Centre, Beijing 100081, China.

Corresponding authors: Bowei Guo (b.guo@ruc.edu.cn); Chenpeng Wang (wangcp@cma.gov.cn).

perienced at least 30 additional days of extreme heat attributable to climate change (Giguere et al., 2025). These heatwaves have profound implications for energy systems, air quality, and human health. Assessments by the IPCC and others suggest that such extremes will increasingly disrupt infrastructure and compound pollution hazards, particularly in densely populated, fossil-fuel-dependent economies (IPCC, 2023; Xu et al., 2023; Cheng et al., 2024; Grant et al., 2025; Zhong et al., 2025). While much research has examined the surge in electricity demand during heat events, far less is known about how extreme heat affects the operational efficiency of power plants and the resulting consequences for air pollution and public health.

Meanwhile, fossil-fuel thermal power plants, still central to electricity supply in many countries, are especially vulnerable to high ambient temperatures under climate change. In 2024, thermal generation accounted for 58.7% of global electricity, with coal-fired plants contributing 34.5% (IEA, 2025). China, the world's largest electricity producer and consumer, relied on thermal power for 61.6% of its generation, 58.4% of which came from coal. Similar patterns prevail in other developing economies: coal-fired shares of electricity reached 84% in South Africa, 72% in India, and 66% in Indonesia (World Bank, 2022). As climate change drives more frequent and severe heatwaves, these coal-dependent power systems face heightened risks of efficiency loss, pollution surges, and adverse health impacts. The intersection of energy security, development, and climate vulnerability thus makes these economies especially exposed to the escalating social and environmental costs of a warming world.

Prior literature has primarily examined demand-driven or atmospheric pathways, or relied on engineering simulations. A critical gap remains: there is still no causal evidence from real-world operations on the efficiency channel. Therefore, in this study, we aim to quantify the extent to which extreme heatwaves affect air pollution by degrading energy use efficiency in the power sector. Specifically, we address two key questions: (1) To what extent do extreme heatwaves increase emissions from the power sector through efficiency losses? (2) What are the resulting social costs of this additional pollution?

To answer these questions, an empirical setting with certain favorable features is particularly useful, including (i) a prolonged and spatially extensive extreme heatwave; (ii) a substantial and diverse fleet of fossil-fuel power plants; and (iii) the availability of high-quality, high-frequency operational, meteorological, and emissions data. While these are not the only conditions under which the efficiency channel could be studied, the summer of 2022 in Guangdong Province satisfies all three. Guangdong is China's most populous province and its largest provincial economy, with over 127 million residents and a GDP of USD 2.1 trillion in 2022, making it a well-suited case for our analysis. That year, Guangdong experienced one of the most severe and prolonged heatwaves on record, with daily maximum temperatures exceeding 38 °C across much of the province.

Leveraging this context, we merge high-frequency operational data from all fossil-fuel power plants in the province with high-resolution weather and emissions measurements, and estimate the causal effect of extreme heatwaves on air pollution through the thermal-efficiency channel. Our difference-in-differences (DID) framework isolates the efficiency-mediated impact of extreme heat on plant-level $PM_{2.5}$ emission intensity, controlling for output variation and meteorological factors. We find that heatwaves raise $PM_{2.5}$ emission intensity by 21.4%

on average, with coal-fired units experiencing an additional 12.3% increase relative to gas-fired units. Similar patterns emerge for other fossil-fuel-related pollutants. Combining these causal estimates with epidemiological concentration-response functions, we attribute over 3,981 premature deaths annually in China to heatwave-induced efficiency losses, corresponding to social costs of USD 4.21 billion. Looking forward, annual costs in China could rise to USD 20.41 billion under the high-emissions SSP5-8.5 scenario, which is associated with approximately 4.4°C warming by 2100. The welfare burden is not uniform: provinces with heavy reliance on coal generation and high population density face disproportionately large damages, whereas hydropower-rich provinces are less affected. Extending the analysis through national and global simulations, we estimate an annual global burden of USD 76.21 billion. Counterfactual fuel substitution from coal to gas could substantially reduce these damages.

Existing research has highlighted several dimensions of the nexus between extreme heat, air pollution, and economic impacts. First, atmospheric science studies confirm that elevated temperatures significantly intensify pollutant formation. For example, Zhang et al. (2017), Yang and Shao (2021), Gao et al. (2024), and Zhong et al. (2025) document notable increases in atmospheric pollutant concentrations during heatwaves, while Jiang et al. (2024) show that each 1°C increase above 27°C sharply raises $PM_{2.5}$ emissions across 2,351 Chinese counties. The closest study to our work is Liu et al. (2024), which uses satellite remote sensing and chemical transport models to detect pollutant spikes near coal-fired power plants during extreme heat. However, these studies largely focus on pollutant concentrations, without directly linking observed changes to operational inefficiencies in power generation.

Second, the interaction of heatwaves and air pollution generates compounding health and economic costs. Epidemiological research shows that concurrent exposure to heat and pollution amplifies cardiovascular and respiratory morbidity (Pope Iii et al., 2002; Schnell and Prather, 2017; Rahman et al., 2022; Xu et al., 2023; Cheng et al., 2024), and emerging evidence points to psychological effects (Zhang et al., 2017; Xie et al., 2023). Labor productivity studies further reveal dual economic losses: heat stress alone depresses industrial productivity (Somanathan et al., 2021), while pollution imposes additional costs (Zivin and Neidell, 2012; He et al., 2019; Chang et al., 2019). For instance, Chang et al. (2016) report an 8% elasticity of productivity loss to $PM_{2.5}$ exposure among U.S. packaging workers, and Fu et al. (2021) find that reducing $PM_{2.5}$ by 1 $\mu g/m^3$ boosts Chinese manufacturing productivity by 0.82%. These findings underscore the broader economic relevance of climate-induced pollution shocks.

Finally, policy-oriented studies have assessed the returns to emissions mitigation. Shen et al. (2025) estimate that every dollar spent on abatement yields $1.10 to $2.45 in health-related benefits globally, with higher returns in densely populated regions with poor air quality. Greenstone et al. (2025) demonstrate that emissions trading markets in India reduce particulate matter by 20–30% while cutting abatement costs by roughly 11%, even under limited regulatory capacity. These insights reinforce the economic rationale for incorporating climate-related externalities into power sector governance.

This study makes three main contributions to the literature. First, it identifies and empirically validates a previously overlooked efficiency channel through which extreme heatwaves elevate air pollution: rather than focusing on demand surges or atmospheric chemistry, we show

that heat stress directly degrades the thermal efficiency of fossil-fuel power plants, thereby amplifying emission intensity. Second, leveraging high-frequency operational, meteorological, and emissions data from all fossil-fuel power plants in Guangdong during the unprecedented 2022 heatwave, we provide the first causal evidence of this mechanism in real-world operations, distinguishing efficiency losses from changes in output or demand. Third, by translating these efficiency-induced emission increases into health and economic damages at the provincial, national, and global scales, we quantify the broader social costs of heatwave-related inefficiencies and demonstrate that cleaner fuel substitution can substantially mitigate these damages.

The remainder of this paper is organized as follows. Section 2 provides institutional background, explaining the thermodynamic mechanisms through which extreme heat impairs fossil-fuel power generation efficiency and introducing the 2022 Guangdong heatwave as our empirical setting. Section 3 describes the data sources, variable construction, and summary statistics. Section 4 presents the empirical identification strategy and the baseline results on heatwave-induced emission intensity, along with heterogeneity and robustness analyses. Section 5 quantifies the social costs associated with efficiency-driven pollution, extending the analysis from China to the global scale and evaluating the welfare implications under alternative climate and policy scenarios. Finally, Section 6 concludes the study.

2 Institutional Background

This section provides a brief background for understanding how extreme heatwaves influence power sector emissions and motivates the choice of our empirical setting. Section 2.1 summarizes the fundamentals of thermal power generation and outlines potential mechanisms through which extreme heat could impair plant efficiency. Section 2.2 then introduces the 2022 extreme heatwave in Guangdong, which forms the basis for our empirical analysis.

2.1 Potential Mechanisms of efficiency degradation under extreme heat

Thermal power generation converts the chemical energy stored in fuels (primarily coal, natural gas, or diesel) into electricity through a sequence of energy transformations. In a coal-fired system, fuel combustion produces high-temperature, high-pressure steam that drives a steam turbine. The turbine converts thermal energy into mechanical energy, which is subsequently transformed into electricity by a generator.

As shown in Figure 1, the coal conveyor (equipment 1) feeds pre-treated coal into the boiler (equipment 2), while the forced draught fan (equipment 6) delivers air for combustion. Inside the boiler, fuel combustion generates high-temperature, high-pressure steam, and the resulting flue gases are discharged through the chimney (equipment 5). The steam drives the steam turbine (equipment 3), which produces mechanical work. The turbine powers the generator (equipment 4), and the resulting electricity is stepped up in voltage and transmitted to the grid via pylons (equipment 9).

Following energy conversion, the exhaust steam enters the condenser (equipment 7), where circulating cooling water condenses it back to liquid form. The warmed water is then sent to the

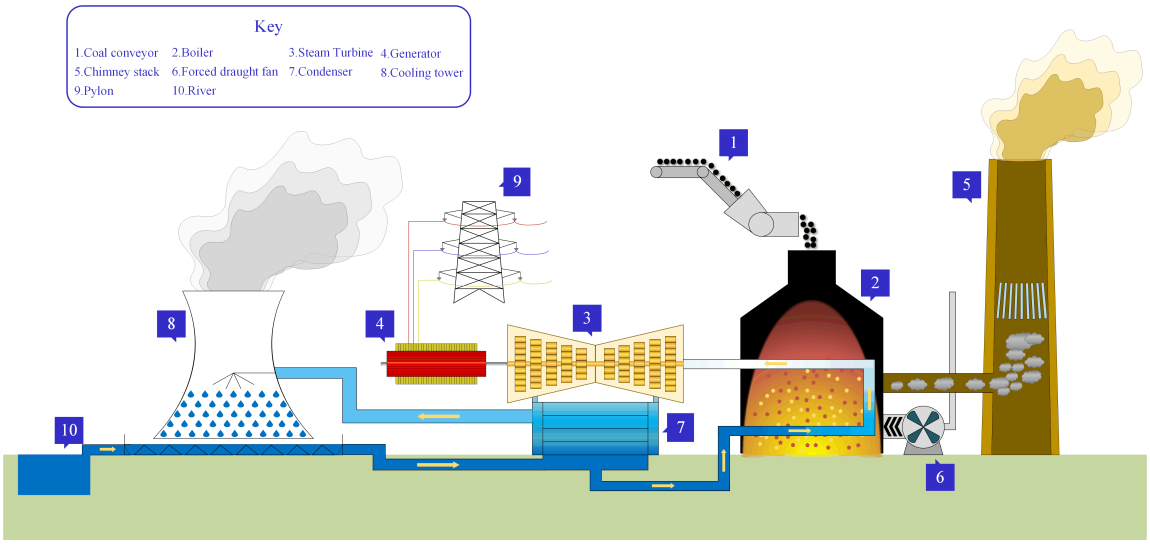


Figure 1: Schematic diagram of a coal-fired power plant

cooling tower (equipment 8), where it releases heat before being reused. Additional water from the river (equipment 10) compensates for evaporative losses, and the condensate is returned to the boiler, completing the thermodynamic cycle.

Extreme heatwaves could potentially impair coal-fired power plant performance through several interrelated pathways. First, reduced cooling efficiency arises because thermodynamic performance depends on the temperature gradient between the heat source (steam) and the heat sink (cooling water). Elevated ambient temperatures reduce the cooling tower's capacity, raising the temperature of circulating water entering the condenser. This narrows the temperature difference with exhaust steam, impairs condensation, increases turbine backpressure, and lowers expansion work. As a result, more fuel must be burned to sustain rated output, leading to higher emissions.

Second, lower combustion efficiency occurs as high ambient temperatures reduce air density, decreasing the oxygen content per unit volume of combustion air supplied by the draught fan. Reduced oxygen availability increases the likelihood of incomplete combustion, lowering energy conversion efficiency and elevating emissions of particulate matter and other incomplete combustion products.

Third, increased auxiliary power demand further aggravates efficiency losses: to compensate for reduced oxygen density, fans must move a larger volume of air, increasing system resistance and auxiliary electricity use. This reduces net output and indirectly requires additional fuel consumption, thereby raising emissions. Fourth, reduced effectiveness of emission control systems also plays a role. Higher flue gas temperatures can push catalysts and absorbents in pollution control devices beyond their optimal operating range, reducing removal efficiency. Even if pollutant formation rates remain constant, diminished control performance increases stack emissions, an effect amplified by higher fuel use.

Finally, coal quality deterioration often accompanies heatwaves, which are typically associated with high humidity. Outdoor coal can absorb moisture and form agglomerates, lowering its heating value and disrupting stable combustion. These effects jointly reduce thermal efficiency

and increase emissions.

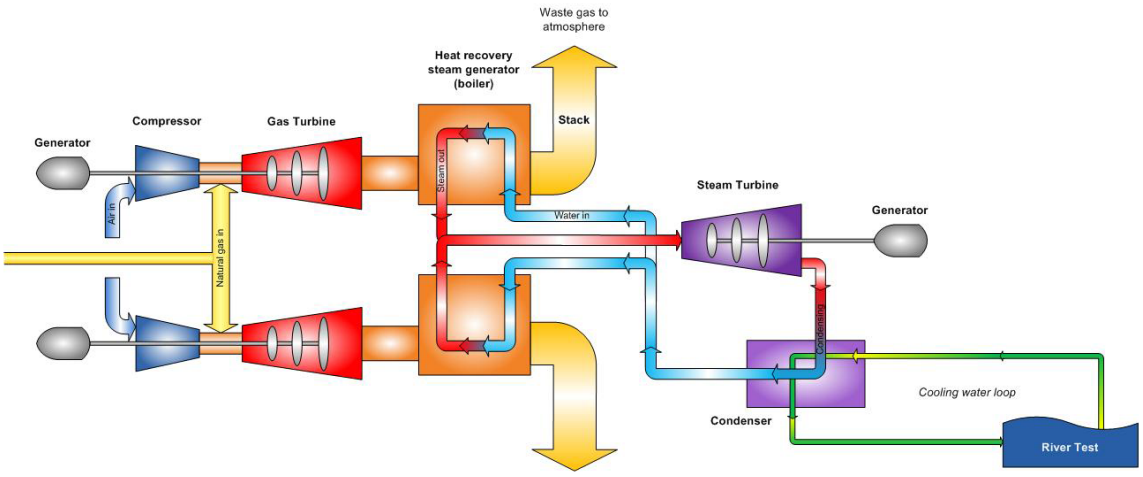


Figure 2: Schematic diagram of a CCGT power plant

Similar to coal-fired power plants, gas-fired generation units are also susceptible to efficiency losses during periods of high ambient temperature. This is especially true for the increasingly prevalent Combined Cycle Gas Turbine (CCGT) systems. As shown in Figure 2, a CCGT unit integrates both a gas turbine and a steam turbine in a cascade configuration to maximize energy utilization. In the gas turbine stage, natural gas combustion produces high-temperature gases that drive the turbine, generating electricity. The hot exhaust gases then enter a Heat Recovery Steam Generator (HRSG), where residual heat is used to produce steam. This steam drives a steam turbine, generating additional electricity. The steam cycle relies on a condenser and associated heat rejection systems, such as cooling towers, to condense exhaust steam and maintain thermodynamic efficiency.

High ambient temperatures can impair both sections of the CCGT system. On the gas turbine side, reduced intake air density requires the compressor to perform additional work to maintain the necessary air mass flow. Elevated temperatures also make it more difficult to cool hot turbine components, lowering thermodynamic efficiency and reducing net power output. On the steam turbine side, heat stress diminishes the performance of cooling systems, raising the temperature of circulating water entering the condenser. This impairs steam condensation, increases turbine backpressure, and reduces expansion efficiency. The combined impact of these effects means that more natural gas must be burned to sustain a given power output, directly increasing emissions of atmospheric pollutants despite the inherently higher baseline efficiency of CCGT units relative to coal-fired plants.

2.2 The 2022 extreme heat event in Guangdong

Between 22 July and 2 August 2022, the core metropolitan areas of Guangdong Province, including Dongguan, Foshan, Guangzhou, and Zhongshan, were affected by an extreme heatwave associated with a persistent subtropical high-pressure system (Figure 3). The event was unprecedented in both duration and intensity, ranking as the most severe heatwave recorded

in the region since 1951. In Guangzhou, the provincial capital, 99.7% of meteorological stations recorded daily maximum temperatures above 35°C, 95.3% exceeded 37°C, and 66.8% surpassed 39°C during this period. Several historical records were broken: on 25 July, a national meteorological station in Guangzhou recorded 39.3°C, tying its previous maximum; the following day set a new record for the highest minimum temperature at 31.1°C. On 29 July, the city reached an exceptional peak of 43.7°C, underscoring the severity of the event.

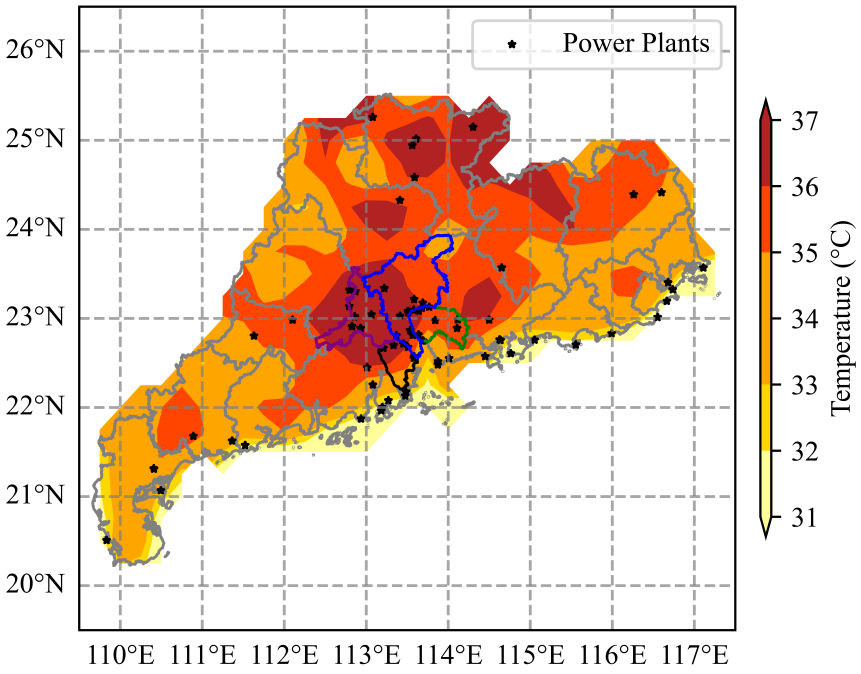


Figure 3: Average daily maximum surface temperature in Guangdong Province during the 2022 heatwave (22 July–2 August)

The heatwave had immediate consequences for both electricity demand and public health. As shown in Figure 4, daily maximum temperature was strongly correlated with electricity generation from fossil-fuel power plants in Guangdong.[1] Electricity output rose sharply with increasing temperature, reflecting the surge in cooling demand and the operational stress imposed on the power sector. At the same time, hospitals in Guangdong reported an increase in heat-related illnesses, particularly strokes among elderly residents.[2] In response, local authorities issued a red alert for high temperatures on 25 July, the first such alert since 2006. They also ordered the suspension of non-essential outdoor work to reduce health risks.[3]

Because most of the province's electricity is generated locally by fossil-fuel power plants, the increase in demand directly translated into higher fossil-fuel-based generation. This shift had notable environmental implications. Figure 5 shows that areas with elevated $PM_{2.5}$ concen-

[1]Due to data unavailability, we are unable to access the daily electricity demand at city level. But the rapid rising demand in Guangdong Province should mainly attribute to the demand from the four affected municipalities because of the extreme heatwave event.

[2]Source: Guangzhou Meteorological Observatory. Climate Impact Assessment for Guangzhou, July 2022. Available at: http://www.tqyb.com.cn/gz/climaticprediction/appraise/2022-08-19/10849.html.

[3]Source: "Guangzhou Issues High-Temperature Red Alert; Electricity Demand Hits Record High." Available at: https://www.caixin.com/2022-07-25/101918345.html.

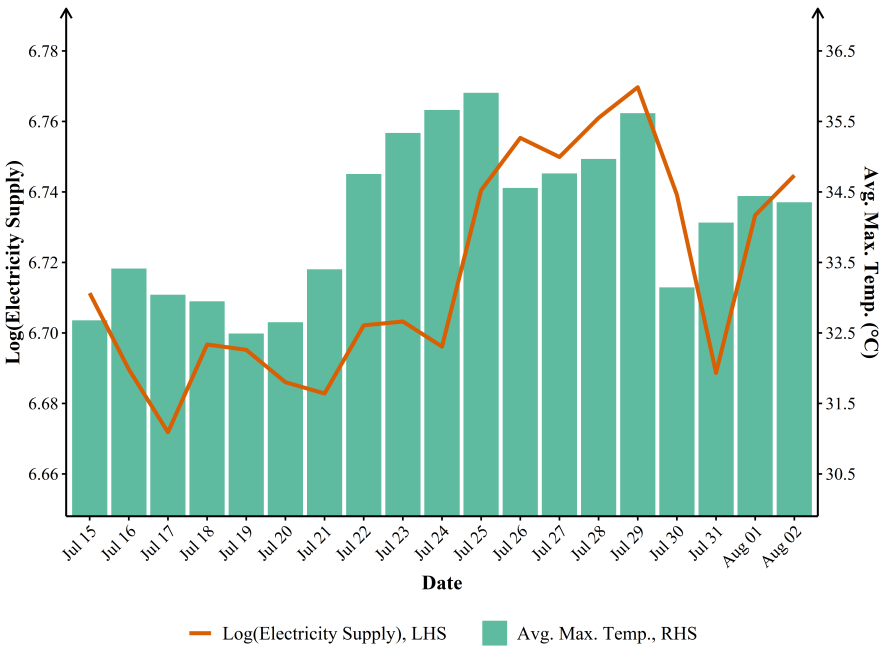


Figure 4: Daily maximum temperature and total electricity generation from fossil-fuel power plants in Guangdong during the heatwave period (22 July–2 August 2022)

trations largely coincide with clusters of fossil-fuel plants, suggesting that intensified electricity generation contributed to the deterioration of air quality. Importantly, many of these plants were also subject to extreme heat during this period, which likely impaired operational efficiency and further increased emissions.

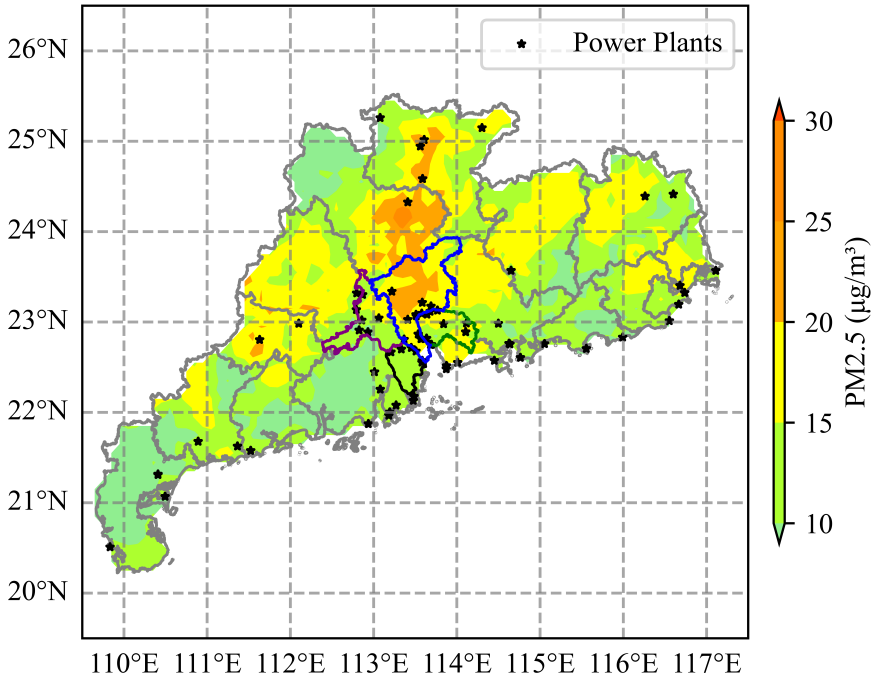


Figure 5: Average $PM_{2.5}$ concentrations in Guangdong Province during the 2022 heatwave (22 July–2 August)

This combination of record-breaking temperatures, elevated electricity demand, and geographically concentrated fossil-fuel generation in the areas most affected by the heatwave offers a unique empirical setting for examining how extreme heat influences thermal power plant efficiency and associated pollutant emissions.

3 Data and Variables

Our analysis draws upon four primary datasets. High-resolution air pollutant data for Guangdong Province during July–August 2022 were obtained from the China Meteorological Administration (CMA). These include daily $PM_{2.5}$ concentrations at a spatial resolution of $0.01^\circ \times 0.01^\circ$ (approximately 1.1 km $\times$ 1.0 km) and daily concentrations of sulfates (SO_4^{2-}), nitrates (NO_3^-), and organic matter (OM) at $0.1^\circ \times 0.1^\circ$ (approximately 11.1 km $\times$ 10.4 km). This fine granularity enables precise alignment between pollutant levels and power plant coordinates, improving attribution of local air quality impacts and reducing confounding from other emission sources and atmospheric transport.

The second dataset contains hourly meteorological observations, also from CMA, covering temperature, wind speed and direction, relative humidity, precipitation, and solar radiation at a spatial resolution of $0.25^\circ \times 0.25^\circ$ (approximately 27.8 km $\times$ 26.1 km). Temperature records are used to identify extreme heatwave episodes, while other meteorological variables control for atmospheric dispersion effects on pollutant concentrations.

The third dataset provides plant-level operational information for all thermal power plants in Guangdong during the same period. It includes hourly generation, nodal prices, fuel type, and installed capacity. These records are central to disentangling increased generation from heat-induced efficiency losses and to examining heterogeneity between coal- and gas-fired units.

Finally, two additional sources inform the estimation of social costs. The Multi-resolution Emission Inventory for China (MEIC) offers province-level pollutant emission estimates across 22 sectors, including power generation. For population exposure modelling, we use the LandScan Global Population Database from Oak Ridge National Laboratory, which provides annual average population distributions on a 30 $\times$ 30 arc-second grid ($\sim$1km $\times$ 1km).

We focus on the period from 15 July to 2 August 2022, which spans the full duration of the extreme heatwave described above. Consistent with standard definitions, an extreme heatwave is identified as at least three consecutive days with maximum daily temperatures exceeding 35°C. The treatment group comprises 28 generating units located in Dongguan, Foshan, Guangzhou, and Zhongshan, which experienced persistent extreme heat beginning 22 July and continuing through 2 August, with only a temporary dip on 30 July (average 33.9°C, still above the 32.3°C recorded in unaffected areas). The control group includes 22 continuously operating units in other Guangdong cities that were not exposed to extreme heat during the same window.

Figure 6 plots the evolution of $PM_{2.5}$ concentrations in areas surrounding power plants in both treatment and control groups. Following the onset of the heatwave on July 22, $PM_{2.5}$ levels near treated plants rose markedly, remained elevated relative to control areas, and only declined after August 1, likely due to weather changes linked to Typhoon Chaba. Despite fluc-

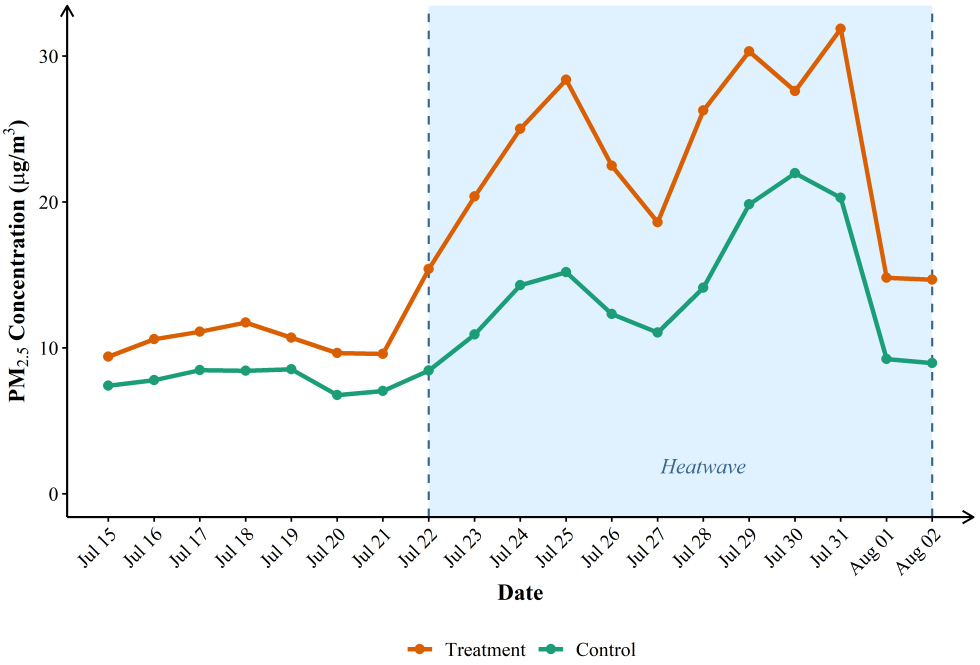


Figure 6: $PM_{2.5}$ concentrations near heatwave-exposed (treatment) and control power plants during the study period

tuations, treated units consistently exhibited higher $PM_{2.5}$ levels, offering suggestive evidence that extreme heat exacerbates pollution from power generation.

Table 1 presents summary statistics for the full sample as well as for treatment and control groups separately. The average $PM_{2.5}$ concentration in the treatment group (18.3 μg/m^3) is substantially higher than in the control group (11.6 μg/m^3), and notable differences are also observed in relative humidity, wind speed, solar radiation, precipitation, maximum daily temperature, and power generation metrics. These contrasts highlight the importance of controlling for meteorological and operational conditions in the empirical analysis.

Table 1: Summary statistics for treatment and control groups

	All			Treatment	Control	Difference
	(1) Mean	(2) Min	(3) Max	(4)	(5)	(6)
$PM_{2.5}$ ($\mu g/m^3$)	15.256	5.200	35.000	18.342	11.634	6.709***
	[7.619]			[8.003]	[5.175]	(15.047)
Relative humidity (%)	79.193	67.552	89.538	77.843	80.779	-2.937***
	[4.690]			[4.786]	[4.038]	(-10.120)
West wind speed (m/s)	0.950	-5.272	7.091	0.613	1.346	-0.733***
	[1.644]			[1.188]	[1.985]	(-7.019)
North wind speed (m/s)	2.802	-0.286	6.759	2.641	2.991	-0.350
	[1.372]			[1.259]	[1.474]	(-3.946)
Solar radiation (W/m^2)	262.573	190.064	313.743	259.127	266.617	-7.490**
	[28.501]			[30.014]	[26.074]	(-4.070)
Precipitation (10^{-5}m)	4.202	0.000	62.500	5.028	3.232	1.795*
	[8.813]			[9.614]	[7.666]	(3.144)
Max day temperature (°C)	34.116	29.547	37.954	35.431	32.572	2.859***
	[2.011]			[1.307]	[1.541]	(30.945)
Power generation (GWh)	80.982	0.261	327.824	47.196	120.645	-73.449***
	[61.128]			[29.181]	[64.911]	(-23.042)
Peak power (MW)	990.235	101.000	3624.000	611.248	1435.133	-823.885***
	[679.694]			[352.167]	[701.805]	(-23.361)
Valley power (MW)	640.089	0.000	3193.000	361.435	967.206	-605.771***
	[554.948]			[259.732]	[626.492]	(-19.979)
Number of plants	50	50	50	28	22	–
Observations	950	950	950	532	418	–

Notes: Columns (1), (4), and (5) report means with standard deviations in brackets. Column (6) reports coefficients from regressions of each variable on the treatment indicator, with t-statistics in parentheses. Significance levels: $^{***}p < 0.01$, $^{**}p < 0.05$, $^{*}p < 0.1$. Decimal places match original data precision.

4 Heatwave Impacts on Emissions

Next, we examine the causal impact of extreme heatwaves on emissions from thermal power plants and unpacks the mechanisms driving these effects. Our analysis proceeds in four steps. Section 4.1 establishes the baseline results, showing that the observed increase in local air pollution near heatwave-exposed plants is not explained by higher electricity output but by a sharp rise in emission intensity, reflecting efficiency losses. Section 4.2 explores heterogeneity across fuel types, documenting that coal-fired plants experience substantially larger efficiency deterioration under extreme heat compared to gas-fired plants. Finally, Section 4.3 conducts a series of robustness checks to ensure that our findings are not driven by alternative explanations.

4.1 Baseline results

We quantify the effect of extreme heatwaves on power plant emissions using a DID framework that exploits plant-level variation in exposure to extreme heat events. The model links high-frequency operational data from all fossil-fuel power plants in Guangdong with high-

resolution meteorological records and continuous emissions monitoring, allowing us to isolate changes in emission intensity attributable to heat stress on plant operations. By focusing on the thermal-efficiency channel, while holding output, fuel type, and broader meteorological conditions constant, this approach recovers the causal effect of heatwaves on pollutant emissions from real-world plant performance rather than from simulations or aggregate correlations. Our primary specification examines $PM_{2.5}$ as a representative pollutant, with robustness checks confirming consistent patterns across other fossil-fuel-related emissions.

The analysis proceeds in two steps. First, we assess whether extreme heat altered generation levels at treated plants. Second, we test whether emission intensity, defined as emissions per unit of electricity generated, increased for treated plants, which would indicate efficiency deterioration.

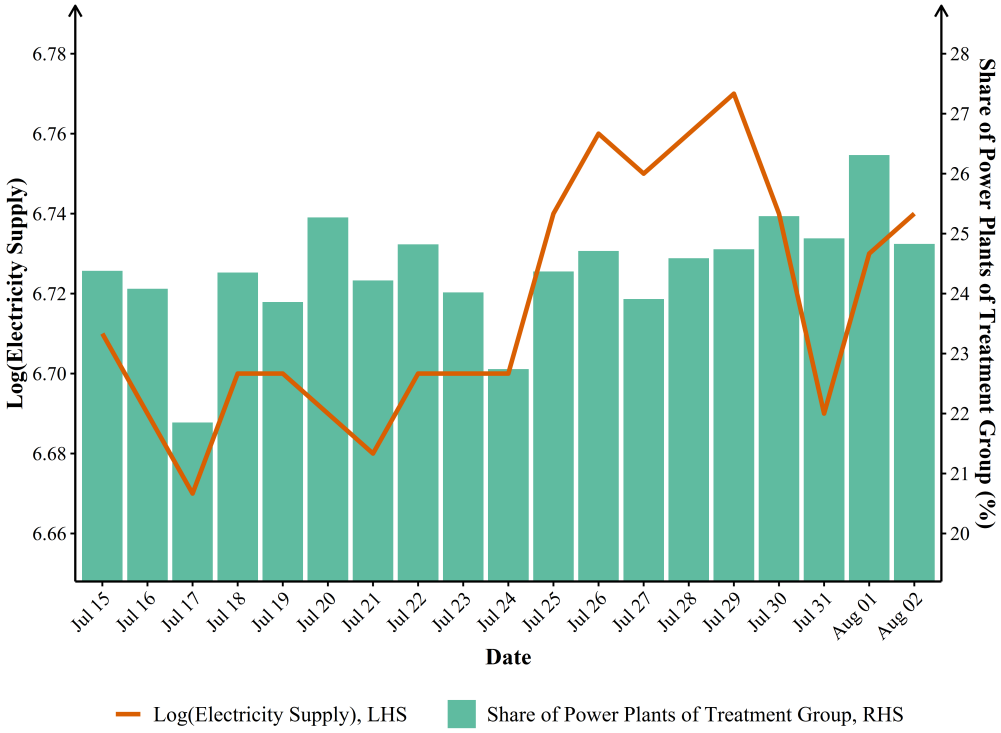


Figure 7: Relative generation share of heatwave-exposed (treatment) power plants during the event window

Although electricity demand surged during the heatwave (as shown in Figure 6), economic dispatch in Guangdong's power market ensures that system-level load increases are allocated based on marginal cost rankings, rather than disproportionately favoring plants located in heat-affected areas with higher local demand. Figure 7 illustrates this argument, showing that the share of total generation supplied by heatwave-exposed plants (treatment group) remains relatively stable throughout the heatwave period, suggesting no major reallocation of dispatch toward these plants.

To formalize this observation, we estimate the following DID specification:

$$\log(Q_{it}) = \delta \cdot 1_{\text{extreme},it} + \alpha Z_{it} + \omega_i + \eta_t + \varepsilon_{it}, \tag{1}$$

where Q_{it} is the electricity generation of plant i on day t; $1_{\text{extreme},it}$ equals 1 if plant i is exposed to extreme heat on day t; Z_{it} includes meteorological controls (temperature bins for non-heatwave days, wind speed, humidity, precipitation, solar radiation); ω_i and η_t denote plant and day fixed effects, respectively. The coefficient δ measures the impact of extreme heat on generation.

Panel A of Table 2 reports the estimates. It shows that once plant and day fixed effects and climate controls are added (columns 2–4), the treatment coefficients are statistically insignificant. This pattern is consistent with Guangdong's market dispatch during the 2022 event: overall system load and total generation rose in response to the heatwave, but the additional output was broadly allocated across the fleet such that the *relative* generation of heatwave-exposed units did not increase compared with unexposed units. Hence, there is no evidence of a differential output response for treated plants in the DID framework.

Given these, the only plausible channel for higher emissions is reduced generation efficiency. Emissions from plant i on day t can be expressed as:

$$E_{it} = e_{it} \cdot Q_{it}, \tag{2}$$

where $e_{it} \equiv E_{it}/Q_{it}$ is emission intensity. Holding Q_{it} constant, any change in E_{it} must originate from e_{it}.

Emission intensity is then estimated as:

$$\log(e_{it}) = \gamma \cdot 1_{\text{extreme},it} + \beta Z_{it} + \theta_i \log(Q_{it}) + \omega_i + \eta_t + \varepsilon_{it}, \tag{3}$$

where γ captures the effect of extreme heat on emission intensity. The term $\log(Q_{it})$ controls for scale effects, and θ_i is allowed to vary across plants to account for heterogeneous operating characteristics.

Panel B of Table 2 presents the results. Across all specifications, extreme heatwaves significantly increase $PM_{2.5}$ emission intensity. In the most saturated model (column 6), the coefficient implies an average increase of about 21.4% in $PM_{2.5}$ emission intensity during heatwaves. The effect is economically meaningful and robust, indicating that the observed rise in local pollution around exposed plants is driven primarily by heat-induced efficiency losses rather than by disproportionate increases in output.

Taken together, these findings confirm that the rise in local air pollution during the heatwave is not driven by higher electricity generation but by a deterioration in generation efficiency, manifested in substantially higher emissions per unit of output. In short, extreme heatwaves significantly compromise thermal power plant efficiency, amplifying environmental externalities through the efficiency channel rather than the output channel.

4.2 Heterogeneity analysis

To estimate the heterogeneity in heatwave-induced efficiency losses between coal- and gas-fired units, we extend the baseline model in Eq. (3) by introducing an interaction term between the heatwave exposure indicator and a coal-plant dummy. This approach allows us to quantify

Table 2: Baseline Estimates: Effects of Extreme Heatwaves on Generation and Emission Intensity

	(1)	(2)	(3)	(4)	(5)	(6)
Panel A: Generation						
Extreme heatwave(=1)	-0.604***	0.020	0.015	0.075	–	–
	(0.051)	(0.041)	(0.047)	(0.067)	–	–
Constant	11.217***	10.997***	11.081***	11.211***	–	–
	(0.034)	(0.015)	(0.522)	(0.519)	–	–
Adjusted R-squared	0.116	0.873	0.872	0.872	–	–
Panel B: Emission Intensity						
Extreme heatwave(=1)	1.326***	0.208***	0.162***	0.122*	0.202***	0.214***
	(0.057)	(0.044)	(0.051)	(0.074)	(0.033)	(0.034)
Constant	4.951***	5.345***	5.039***	5.046***	16.308***	16.616***
	(0.036)	(0.017)	(0.595)	(0.607)	(0.348)	(1.194)
Adjusted R-squared	0.346	0.907	0.907	0.908	0.987	0.987
Observations	950	950	950	950	950	950
Day FE	NO	YES	YES	YES	YES	YES
Plant FE	NO	YES	YES	YES	YES	YES
Climate Control	NO	NO	YES	YES	YES	YES
Temperature Box	NO	NO	NO	YES	YES	YES
Generation Control	NO	NO	NO	NO	YES	YES
Plant*Quantity FE	NO	NO	NO	NO	NO	YES

Notes: Robust standard errors in parentheses: $^{***}p < 0.01$, $^{**}p < 0.05$, $^{*}p < 0.1$. Panel A uses plant-level generation output as the dependent variable. Panel B uses plant-level emission intensity as the dependent variable. Column (1) reports the unconditional association between extreme heatwaves and outcomes without fixed effects or controls. Column (2) introduces day and plant fixed effects to account for time-invariant plant heterogeneity and common shocks. Column (3) further controls for time-varying climate variables (e.g., precipitation, humidity). Column (4) additionally incorporates a flexible temperature-box specification to capture nonlinear responses. Column (5) adds generation controls to isolate changes in emission intensity that are not mechanically driven by output variation. Finally, column (6) includes plant-by-quantity fixed effects, providing the most stringent specification by absorbing variation in plant-specific generation levels over time.

not only the average effect of extreme heat on operational efficiency but also the differential impact attributable to fuel type. Formally, we estimate:

$$\log(e_{it}) = \gamma_1 \cdot 1_{\text{extreme},it} + \gamma_2 \cdot 1_{\text{extreme},it} \times 1_{\text{coal},i} + \beta Z_{it} + \theta_t \log(Q_{it}) + \omega_i + \eta_t + \varepsilon_{it}, \quad (4)$$

where $1_{\text{coal},i}$ equals 1 for coal-fired plants and 0 otherwise. The coefficient γ_1 measures the effect of extreme heat on gas-fired plants (the reference category), while γ_2 captures the additional effect for coal-fired units. Given the greater steam-cycle sensitivity and cooling demands of coal-fired technology, we expect $\gamma_2 > 0$, indicating that coal-fired plants experience larger operational efficiency penalties under extreme heat compared with gas-fired counterparts, all else being equal.

The results are reported in Table 3. Panel A shows that, consistent with the baseline results, extreme heatwaves do not significantly alter generation among affected units relative to unaffected ones once we control for plant and time fixed effects, climate conditions, and operational

Table 3: Heterogeneity Analysis: Interaction Between Extreme Heatwaves and Fuel Type

	(1)	(2)	(3)	(4)	(5)	(6)
Panel A: Generation						
Extreme heatwave(=1)	-0.018	-0.016	0.039	0.131	–	–
	(0.058)	(0.062)	(0.078)	(0.133)	–	–
Extreme × Coal	0.085	0.067	0.083	-0.049	–	–
	(0.056)	(0.055)	(0.053)	(0.121)	–	–
Constant	10.996***	11.059***	11.202***	10.807***	–	–
	(0.015)	(0.521)	(0.520)	(0.717)	–	–
Adjusted R-squared	0.873	0.872	0.872	0.874	–	–
Panel B: Emission Intensity						
Extreme heatwave(=1)	0.246***	0.191***	0.149*	0.002	0.139***	0.145***
	(0.061)	(0.065)	(0.084)	(0.134)	(0.037)	(0.039)
Extreme × Coal	-0.083	-0.063	-0.062	0.147	0.097***	0.123***
	(0.059)	(0.057)	(0.056)	(0.124)	(0.035)	(0.040)
Constant	5.345***	5.060***	5.053***	5.823***	16.677***	17.114***
	(0.017)	(0.594)	(0.607)	(0.786)	(0.384)	(1.215)
Adjusted R-squared	0.907	0.907	0.908	0.909	0.987	0.987
Observations	950	950	950	950	950	950
Climate Control	NO	YES	YES	YES	YES	YES
Temperature Box	NO	NO	YES	YES	YES	YES
Temperature Box × Coal	NO	NO	NO	YES	YES	YES
Generation Control	NO	NO	NO	NO	YES	YES
Plant × Quantity FE	NO	NO	NO	NO	NO	YES

Notes: Robust standard errors in parentheses. $^{***}p < 0.01$, $^{**}p < 0.05$, $^{*}p < 0.1$. Panel A uses plant-level generation output as the dependent variable. Panel B uses plant-level emission intensity as the dependent variable. Columns (1)–(6) progressively add fixed effects and controls, as in Table 2. Table 3 extends this specification by interacting the heatwave indicator with plant types.

constraints. The interaction terms between heatwave exposure and coal-fired status are statistically insignificant across all specifications, indicating that coal and gas units exhibit broadly similar generation responses to heat stress.

Panel B provides evidence of heterogeneity in emission intensity. In the fully specified model (column 6), heatwave exposure increases emission intensity by 14.5% for gas-fired plants. The interaction term between heatwave exposure and coal-fired status is positive and significant, indicating an *additional* 12.3% increase in emission intensity for coal units. Together, these effects imply that coal-fired plants experienced an overall efficiency-related emission surge exceeding 26.8% during the heatwave. This difference aligns with engineering expectations: coal boilers are more vulnerable to air density reductions and cooling system inefficiencies under extreme heat, whereas gas plants exhibit greater thermal resilience, particularly those with combined-cycle configurations.

4.3 Robustness checks

We conduct a series of robustness tests to validate our core finding that extreme heatwaves cause substantial efficiency losses in fossil-fuel power plants, leading to elevated emissions.

First, we verify that our results are not specific to $PM_{2.5}$ by examining three additional pollutants, particularly organic matter (OM), sulfates (SO_4^{2-}), and nitrates (NO_3^-). These pollutants are strongly linked to fossil-fuel combustion. OM typically accounts for 20%–50% of $PM_{2.5}$ mass (Wang et al., 2020), while SO_4^{2-} and NO_3^- form as secondary aerosols from sulfur and nitrogen oxides emitted during combustion. Thermal power plants contribute 15.5% and 18.9% of annual SO_4^{2-} and NO_3^- emissions in China, respectively (Geng et al., 2024).

To conduct the analysis, the dependent variable in Eqs (3) and (4), $\log(e_{it})$, represents the emission intensity for these additional pollutants. The results are shown in Table 4, suggesting that extreme heatwaves substantially increase the emission intensity of all three pollutants. For OM, SO_4^{2-}, and NO_3^-, heatwave exposure raises emissions by 29.5%, 33.1%, and 39.0%, respectively. The inclusion of interaction terms with fuel type reveals that these increases are concentrated in coal-fired plants, whose emissions rise by an additional 25.4%, 28.6%, and 23.3% relative to gas-fired plants. These results demonstrate that the efficiency-driven pollution surge documented earlier generalizes across multiple pollutants closely linked to fossil-fuel combustion, and is particularly pronounced for coal-fired generation units.

Table 4: Robustness Test: Effects of Extreme Heatwaves on Other Pollutants

	OM		SO_4^{2-}		NO_3^-	
	(1)	(2)	(3)	(4)	(5)	(6)
Emission Intensity						
Extreme heatwave(=1)	0.295***	0.137	0.331***	0.156*	0.390***	0.248***
	(0.084)	(0.087)	(0.081)	(0.084)	(0.092)	(0.090)
Extreme treatment × Coal		0.254***		0.286***		0.233**
		(0.097)		(0.094)		(0.099)
Constant	8.071***	9.333***	7.503***	8.793***	7.302**	8.385***
	(2.842)	(2.951)	(2.685)	(2.777)	(2.944)	(3.080)
Adjusted R^2	0.933	0.933	0.939	0.939	0.922	0.922
Observations	950	950	950	950	950	950

Notes: Robust standard errors in parentheses. $^{***}p < 0.01$, $^{**}p < 0.05$, $^{*}p < 0.1$. This table tests robustness by replacing the dependent variable with alternative pollutant emission intensities, including organic matter (OM), sulfate (SO_4^{2-}), and nitrate (NO_3^-). Odd-numbered columns report baseline effects of extreme heatwaves, while even-numbered columns additionally include an interaction term with coal-fired plants to capture heterogeneous impacts by fuel type. All control variables shown in Tables 2 and 3 are included.

Second, we test the sensitivity of our pollution-matching approach by expanding the averaging radius for $PM_{2.5}$ from 1 km (baseline) to 10 km. Results in Columns (1) and (2) of Table 5 indicate that coefficients decline by approximately 6.4% relative to baseline. This pattern is consistent with the expected dilution of pollutants over larger distances, but the estimates remain statistically significant.

Next, to address concerns that emissions from nearby industrial facilities could bias estimates, we visually inspect high-resolution satellite imagery from Google Maps. Among 28 treated plants, 7 are adjacent to industrial sites, none with visible smokestacks. In the control group, 4 of 22 plants have nearby facilities, with only one showing observable emission infrastructure. Excluding these plants yields results consistent with the baseline (Columns (3)–(4) of Table 5).

Furthermore, we reconstruct emission intensity using only $PM_{2.5}$ concentrations above the safe threshold defined by Burnett et al. (2018) (2.4 $\mu g/m^3$), rather than total $PM_{2.5}$. Results (Columns (5)–(6) of Table 5) remain consistent, further confirming robustness.

Table 5: Robustness Check: Alternative Spatial Matching and Exclusion of Industrial Neighbors

	Alt. spat. mtch.		Excl. indust. neighb.		Alt. emiss. intens. meas.	
	(1)	(2)	(3)	(4)	(5)	(6)
Emission Intensity						
Extreme treatment (=1)	0.278***	0.101	0.230***	0.130***	0.212***	0.134***
	(0.080)	(0.081)	(0.039)	(0.043)	(0.043)	(0.047)
Extreme × Coal		0.295***		0.154***		0.146***
		(0.095)		(0.044)		(0.049)
Constant	9.639***	11.039***	16.713***	17.459***	16.418***	17.031***
	(2.612)	(2.712)	(1.441)	(1.462)	(1.556)	(1.582)
Adjusted R-squared	0.940	0.940	0.988	0.988	0.982	0.982
Observations	950	950	741	741	950	950

Notes: Robust standard errors in parentheses. $^{***}p < 0.01$, $^{**}p < 0.05$, $^{*}p < 0.1$.

Finally, we conduct placebo tests to rule out bias from unobserved confounders or model misspecification. We randomly assign pseudo-treatment status to plants and simulate 500 synthetic "placebo heatwave shocks," re-estimating the baseline model each time.

Figure 8 plots the distribution of placebo estimates. The kernel density centers around zero, with a symmetric shape approximating normality, indicating no systematic relationship under random assignment. Over 96% of simulated p-values exceed the 1% threshold, and fewer than 4% fall below it. Moreover, effect sizes from outliers never exceed 6.5%, substantially smaller than the actual baseline estimate of 21.4%. These findings confirm that results are unlikely to be driven by chance or omitted variable bias.

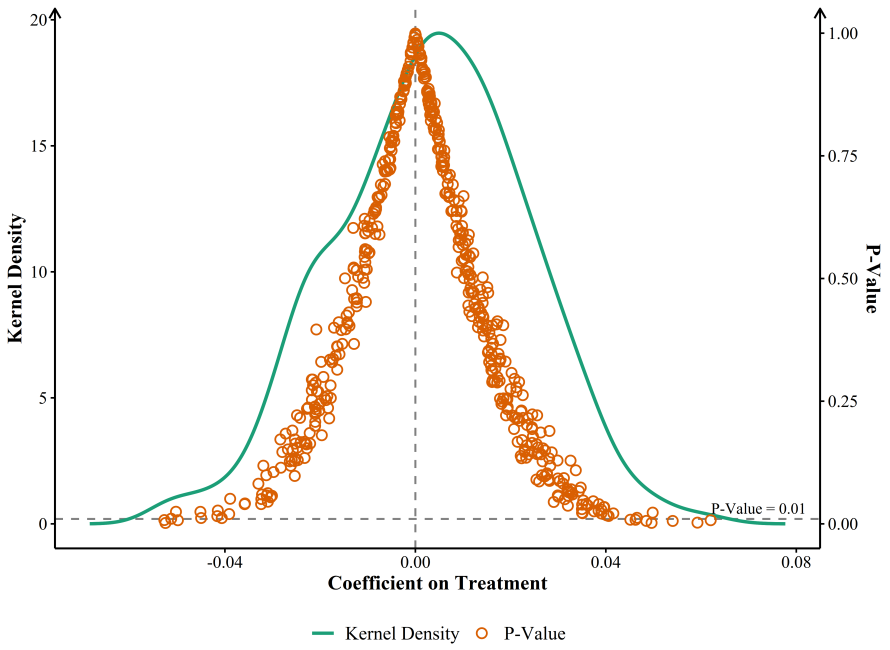


Figure 8: Distribution of estimated heatwave effects from 500 random placebo assignments

5 Social Costs of Heatwave-Induced Pollution

Extreme heatwaves not only impair the operational efficiency of fossil-fuel power plants but also translate these efficiency losses into tangible welfare damages through elevated emissions and air pollution exposure. This section quantifies the economic and health costs arising from heatwave-induced pollution, integrating engineering-based efficiency estimates with epidemiological concentration-response models. We first develop an estimation strategy that links plant-level efficiency deterioration to marginal changes in pollutant concentrations, mortality risks, and their monetized social costs. We then apply this framework to China, assessing provincial disparities and temporal dynamics under alternative climate scenarios. Extending the analysis globally, we evaluate the cross-country distribution of welfare burdens and identify regions most vulnerable to efficiency-driven pollution shocks. Finally, we discuss policy implications and counterfactual substitution scenarios, highlighting how cleaner fuel structures can mitigate the social costs of extreme heat in a warming world.

5.1 Estimation strategy

We quantify the welfare implications of heatwave-induced efficiency losses by linking plant-level operational impacts to population health damages through a two-step marginal damage valuation framework. Extreme heat raises fuel use per unit of electricity output, increasing emissions of air pollutants. These emissions contribute to ambient concentrations that affect human health via well-documented exposure-response relationships, and can be monetized using standard valuation metrics.

First, we attribute changes in pollutant concentrations specifically to the heat-induced emis-

sion increase from fossil-fuel power plants. Following Greenstone et al. (2025), national baseline concentrations are scaled by the electricity sector's contribution share and the percentage increase in emissions derived from regression results:

$$z_{jk} = z_{jk}^{\text{base}} \times \left(1 + \beta_k \cdot r_{jk}\right), \tag{5}$$

where z_{jk}^{base} is the baseline concentration of pollutant k in country j, β_k is the sector's share of emissions for pollutant k, and r_{jk} is the percentage increase in emissions from fossil-fuel plants due to heat-induced efficiency losses (estimated as the regression coefficients from Section 4). This formulation isolates the marginal pollution attributable to the efficiency channel.

Second, we translate these incremental concentration changes into mortality risks. For $PM_{2.5}$, we use the Global Exposure Mortality Model (GEMM) (Burnett et al., 2018), which captures nonlinear exposure-risk relationships across major disease endpoints, including lower respiratory tract infections (LRTI), chronic obstructive pulmonary disease (COPD), lung cancer, ischemic heart disease (IHD), and stroke:

$$RR_h(z_{\text{PM}_{2.5}}) = \exp\left(\beta_h \cdot \frac{\log\left(1 + \frac{\Delta z_{\text{PM}_{2.5}}}{\alpha_h}\right)}{1 + \exp\left(-\frac{\Delta z_{\text{PM}_{2.5}} - \mu_h}{\nu_h}\right)}\right), \tag{6}$$

where $\Delta z_{\text{PM}_{2.5}} \equiv \max(z_{\text{PM}_{2.5}} - z_{\text{PM}_{2.5}}^{cf}, 0)$ and $z_{\text{PM}_{2.5}}^{cf} = 2.4\ \mu\text{g/m}^3$ is the counterfactual threshold. Parameters α_h, β_h, μ_h, and ν_h are from Burnett et al. (2018). For sulfates (SO_4^{2-}) and nitrates (NO_3^-), we adopt the linear relative risk model from Orellano et al. (2021):

$$RR_{hk}(z_k) = \exp\left(\delta_{hk} \cdot \max(z_k - z_k^{cf}, 0)\right), \tag{7}$$

where δ_{hk} is the pollutant-specific risk coefficient and z_k^{cf} is the no-harm threshold.

The number of premature deaths attributable to pollutant k and disease h in country j is then computed using the Global Burden of Disease (GBD) framework (Cohen et al., 2017):

$$M_{jhk} = \gamma_{0,h} \cdot \text{pop}_j \cdot \left[\frac{RR_h(z_{jk}^{EH}) - 1}{RR_h(z_{jk}^{EH})} - \frac{RR_h(z_{jk}^{base}) - 1}{RR_h(z_{jk}^{base})}\right], \tag{8}$$

where $\gamma_{0,h}$ is the baseline mortality rate for disease h, and pop_j is the exposed population. The bracketed term isolates the marginal health risk due to heatwave-induced emissions. Notably, h includes lower respiratory tract infections (LRTI), chronic obstructive pulmonary disease (COPD), lung cancer, ischemic heart disease (IHD), and stroke.

Finally, we monetize mortality impacts using the VSL, adjusted for income differences following the World Bank and IHME (2016) method:

$$\text{VSL}_j = \text{VSL}_{\text{OECD}} \left(\frac{Y_j}{Y_{\text{OECD}}}\right)^{\varepsilon},$$

where VSL_{OECD} is set at \$3.83 million (2011 USD), Y_{OECD} is the OECD average per capita

GDP ($37,000), Y_j is the per capita GDP of country j, and ε is the income elasticity of VSL, assumed to be 1.2. Social costs are then expressed as:

$$SC_j = VSL_j \cdot \sum_h \sum_k \zeta_k \cdot M_{jhk}, \tag{9}$$

where ζ_k scales mortality-based estimates to total social costs by accounting for morbidity, productivity, and other non-mortality effects. We adopt scaling factors from Muller and Mendelsohn (2007), which indicate mortality shares of 82.76% for $PM_{2.5}$, 82.56% for SO_4^{2-}, and 70.97% for NO_3^-.

To translate estimated emission increases into monetary damages, we parameterize the social cost calculations under three complementary scopes: provincial-level estimates within China, multi-year national estimates for China, and cross-country global estimates. The core approach relies on mortality-related damages from elevated $PM_{2.5}$, SO_2, and NO_2 concentrations. To obtain comprehensive measures of total social costs, these mortality damages are expanded using pollutant-specific scaling factors drawn from the literature, which indicate that premature mortality typically accounts for 70–83% of the overall damages (Muller and Mendelsohn, 2007).

Our framework accounts for substantial heterogeneity across provinces, including variation in extreme heat exposure, baseline emissions, generation mix, and population vulnerability. To capture regional differences in heatwave intensity, we calculate the average duration of extreme heat events within each province, providing a metric that highlights spatial disparities in exposure. Mortality damages are then estimated using concentration-response functions from the Global Burden of Disease (GBD) study and monetized with a uniform China-specific VSL. Finally, these mortality damages are scaled by pollutant-specific adjustment factors to approximate the full range of social costs attributable to heatwave-induced efficiency losses in the power sector.

To assess persistence, we extend the analysis across multiple years using historical climate and generation records. Excess emissions are computed by applying regression-derived deterioration coefficients to observed national thermal generation during extreme heat events in recent years. Annual mortality damages are monetized using the same uniform China-specific VSL, in line with recent integrated assessment practice, and subsequently scaled to derive total social costs. This procedure allows us to capture interannual variability in the economic burden of pollution-related damages from extreme heat.

For the global analysis, we quantify each country's exposure to heatwave days using the ERA5 reanalysis dataset. For every $0.25^\circ \times 0.25^\circ$ grid cell worldwide, we count the number of days in 2022 when maximum temperature exceeded 35°C, and then compute the area-weighted national sum of such days. To validate these measures, we compare them with publicly reported exposure-day statistics and find broad consistency. Country-level emissions are drawn from the Emissions Database for Global Atmospheric Research (EDGAR), electricity generation by fuel type from the U.S. Energy Information Administration (EIA), and pollutant exposures from the State of Global Air ($PM_{2.5}$, NO_2) and ECMWF's Atmospheric Composition Reanalysis 4 (SO_2). Mortality impacts are estimated using GBD functions and monetized under two

scenarios: one applying a uniform China-specific VSL, and another applying country-specific VSL adjustments. Our sample covers 137 countries, representing approximately 95% of the global population, thereby enabling a comprehensive assessment of the worldwide burden of heatwave-induced efficiency losses.

5.2 Welfare Burden in China

Figure 9 quantifies the resulting social costs across Chinese provinces, accounting for heterogeneous local conditions. Coastal and industrially concentrated provinces such as Zhejiang, Henan, Jiangsu, and Guangdong exhibit the largest efficiency-induced increases in pollutant emissions, reflecting both their higher baseline reliance on coal-fired generation and the intensified pressure resulting from more severe rises in ambient temperatures. In contrast, provinces with larger shares of hydropower and renewables (e.g., Yunnan, Sichuan) experience more muted effects, as thermal units play a smaller role in balancing system demand. Provinces located in the northeastern and northwestern regions (such as Heilongjiang, Jilin, Liaoning, Qinghai, Ningxia, and Gansu), experience comparatively smaller social costs. This can be attributed to their shorter exposure duration to extreme heat. The spatial divergence highlights that the welfare costs of heatwaves are not uniformly distributed but instead cluster in regions where fossil-based generation dominates and population exposure is greatest.

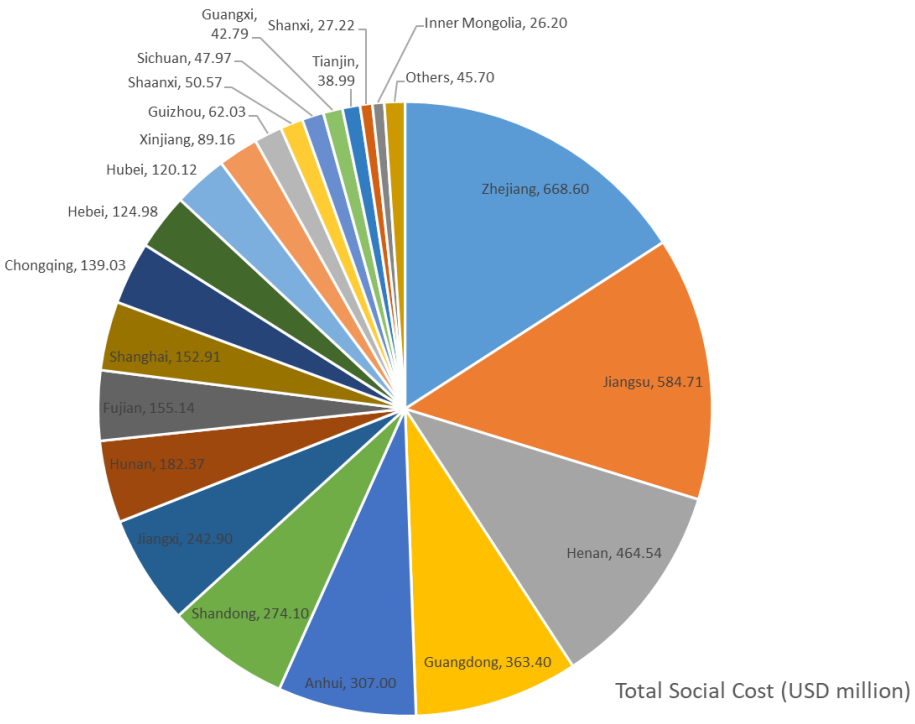


Figure 9: Provincial-level estimates of heatwave-induced increases in emission intensity across China

We next approximate the aggregate welfare burden that heatwave-induced efficiency losses impose on the country as a whole. The results demonstrate that excess $PM_{2.5}$, sulfate (SO_4^{2-}),

and nitrate (NO_3^-) emissions are associated with approximately 3,981 premature deaths annually. Applying a China-specific value of statistical life (VSL) of USD 1.06 million yields a total social cost of USD 4.21 billion per year. To ensure robustness, we employ two alternative methodologies to estimate China's social costs in Appendix A, both yielding highly consistent estimates.

We also assess how these welfare costs have evolved historically under the assumption that extreme heatwaves impose uniform efficiency losses on fossil-fuel power plants nationwide. Figure 10 shows the estimated trajectory of overall social costs in China over the past 22 years, calculated by aggregating province-level estimates weighted by each province's extreme heatwave duration. Prior to 2014, the annual social costs of excess pollutant emissions remained in the range of USD 8–9 billion, but they have declined markedly over the past decade. On a per-unit basis, the social cost of thermal power generation fell from USD 143/MWh in 2002 to USD 13/MWh in 2024. This represents a 90% reduction over two decades. The downward trend is largely driven by the substantial decline in ambient pollution levels in China, which lowers the health damages associated with marginal emissions from power plants. Notably, the 2024 value amounts to 13% of the average off-peak grid purchase price of electricity across Chinese provinces in July 2024, highlighting the continued, though diminishing, burden of pollution-related damages in the power sector.

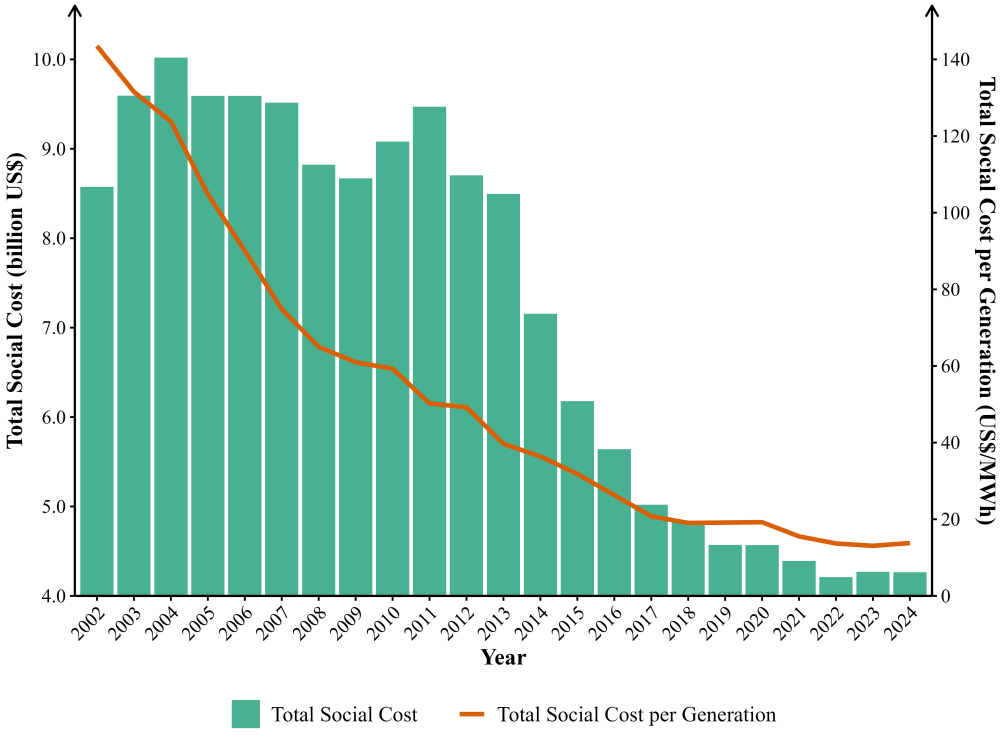


Figure 10: Historical evolution of social costs associated with heatwave-induced efficiency losses in China

Figure 11 illustrates the temporal evolution of pollutant-specific contributions to social costs in China. Nitrate (NO_3^-) has consistently dominated, accounting for 77.0%–86.0% of the total, while $PM_{2.5}$ and sulfate (SO_4^{2-}) contribute smaller shares of 10.8%–18.9% and 3.1%–4.3%,

respectively. This reflects the central role of NO_3^- in driving health-related damages from heat-induced efficiency losses.

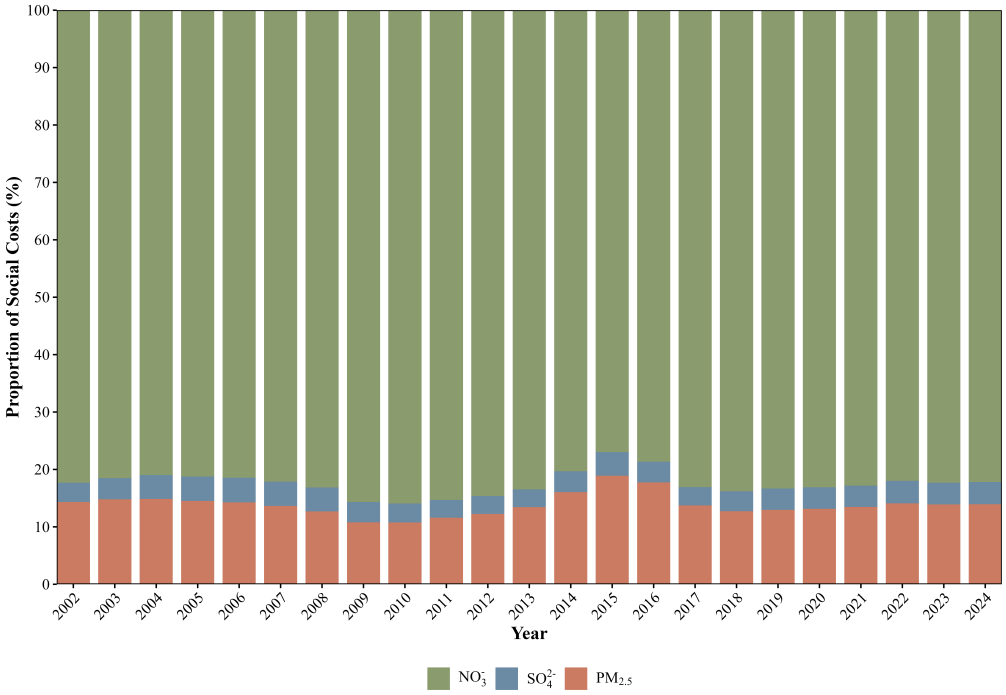
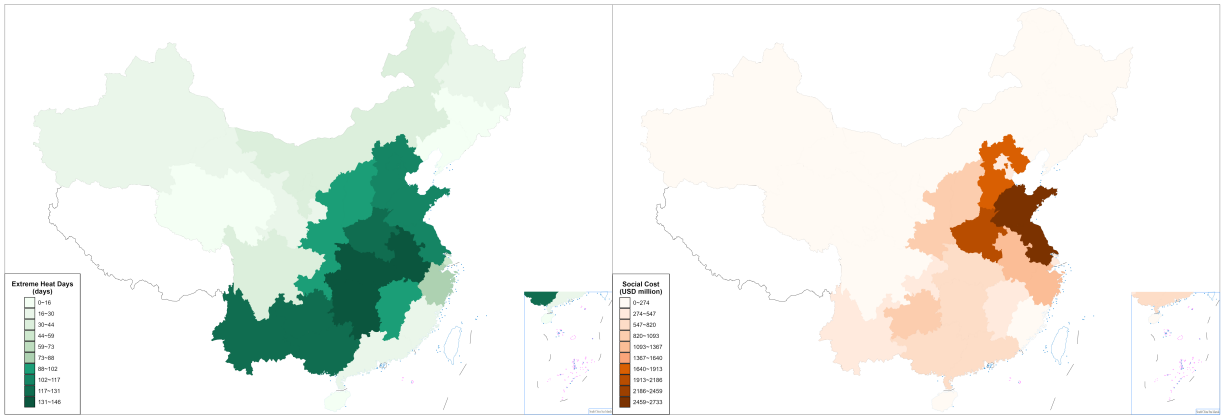


Figure 11: Pollutant contribution to the evolution of total social costs in China over time

Furthermore, climate change is projected to substantially exacerbate these costs. Under a high-emission scenario (SSP5–8.5), China's annual social cost could rise to USD 20.41 billion. These costs are unevenly distributed across provinces, reflecting heterogeneity in climate deterioration, electricity generation composition, and population size. Figure 12a shows the projected number of hot days above 35°C, while Figure 12b presents the corresponding provincial social costs under SSP5–8.5. On average, provinces experience 83.7 extreme heat days annually, with central provinces (Hunan, Hubei, Henan, Shandong), southwestern regions (Guizhou, Yunnan), and several southeastern coastal provinces (Anhui, Guangxi, Jiangsu) facing the most severe outcomes—exceeding 110 days per year. In contrast, northwestern, northeastern, and some southeastern coastal provinces (e.g., Guangdong, Fujian) experience fewer than 40 such days. Under this climate change scenario, total social costs reach approximately USD 20.41 billion, concentrated in Shandong, Jiangsu, Henan, Hebei, Anhui, and Zhejiang, each exceeding USD 1 billion. For comparison, under a medium-emission scenario (SSP2–4.5) and a low-emission scenario (SSP1–2.6), China's annual social costs are projected at USD 12.50 billion and USD 12.37 billion, respectively, which are still around three times the present-day estimate (see Appendix B for details). These projections underscore the urgency of accelerated mitigation efforts to limit warming and reduce future social costs.



(a) Projected number of hot days in each province (b) Estimated social costs across provinces

Figure 12: Projected provincial outcomes under the SSP5–8.5 high-emissions scenario.

5.3 Global distribution and cross-country heterogeneity

Extending the analysis to the global scale, and applying country-specific extreme heat frequencies, generation mixes, and baseline concentration of pollutants, we estimate that efficiency-related emission increases cause approximately 63,932 premature deaths per year, corresponding to a social cost of USD 76.21 billion, representing approximately 7.55 per ten thousand (‰) of global GDP in 2022 (USD 101 trillion). The distribution of this burden is highly skewed: as shown in Figure 13, the ten most affected countries (India, China, Pakistan, Iraq, Egypt, Iran, Bangladesh, Syria, Saudi Arabia, and Yemen) account for 93.33% of global mortality. India alone bears 47,885 deaths annually (74.90% of the total), followed by China with 3,336 deaths (5.22%). Despite substantial progress in air quality control, China's large population and coal-heavy generation mix magnify its vulnerability.

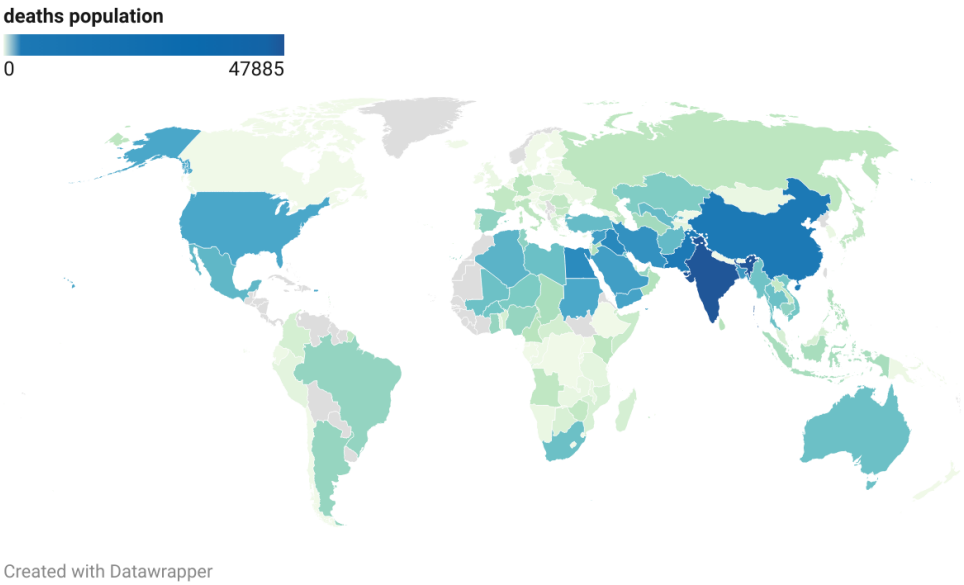


Figure 13: Global distribution of premature deaths from heatwave-induced efficiency losses in the power sector

These mortality patterns translate into highly concentrated economic losses (Figure 14). Using the global average VSL of USD 1.19 million, we find that India accounts for USD 76.21 billion in annual damages. Together, the top ten countries capture more than 90% of global welfare losses from this channel. This concentration underscores the disproportionate vulnerability of populous, coal-dependent economies to climate-sensitive efficiency shocks in the power sector. We also use country specific VSL, and the results are presented in Appendix C in the Supplementary Information.

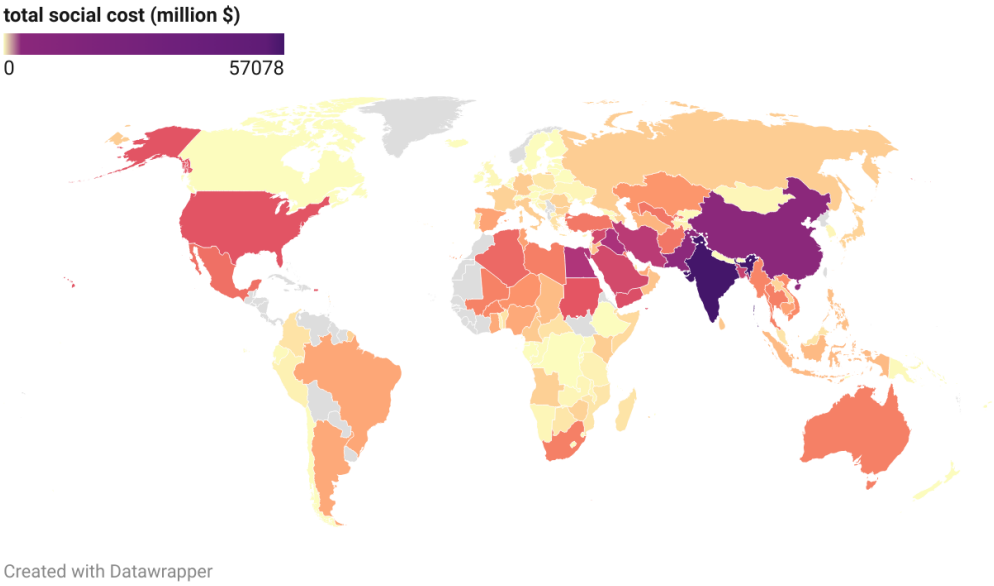


Figure 14: Global distribution of social costs from heatwave-induced efficiency losses in the power sector

Figure 15 further presents pollutant-specific contributions to social costs across the top ten most affected countries (under uniform VSL). In nearly all cases, NO_3^- is again the largest contributor, followed by $PM_{2.5}$, with SO_4^{2-} playing only a minor role. The relative magnitudes, however, vary significantly across countries, reflecting differences in baseline pollutant concentrations, atmospheric chemistry, and population exposure levels.

5.4 Policy Implications and Counterfactual Scenarios

Replacing coal-fired generation with gas-fired plants is an important step toward building a modern power system that balances supply security with green transformation. In 2024, China's installed natural gas generation capacity reached 143.67 million kW, accounting for 9.95% of national thermal capacity. Yet, annual output was only 317.12 billion kWh (or 4.98% of thermal generation), reflecting persistently high generation costs.

During extreme heat periods, however, our results demonstrate that efficiency losses for gas-fired units are substantially smaller than those for coal-fired plants. Building on this, we simulate a gas-for-coal substitution strategy in which all coal-fired units are replaced by gas-fired units, and estimate the corresponding reduction in social costs induced by heatwave-related efficiency losses.

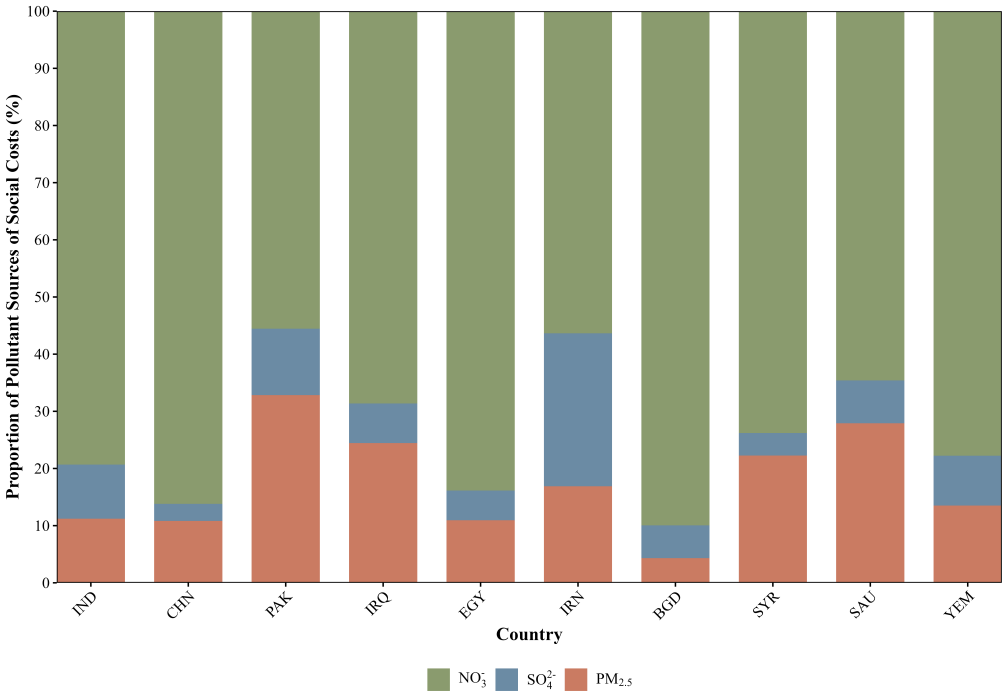


Figure 15: Pollutant contribution to total social costs across the top ten countries. Although NO_3^- dominates overall, the relative shares of $PM_{2.5}$ and SO_4^{2-} differ across countries, reflecting local atmospheric and energy system conditions.

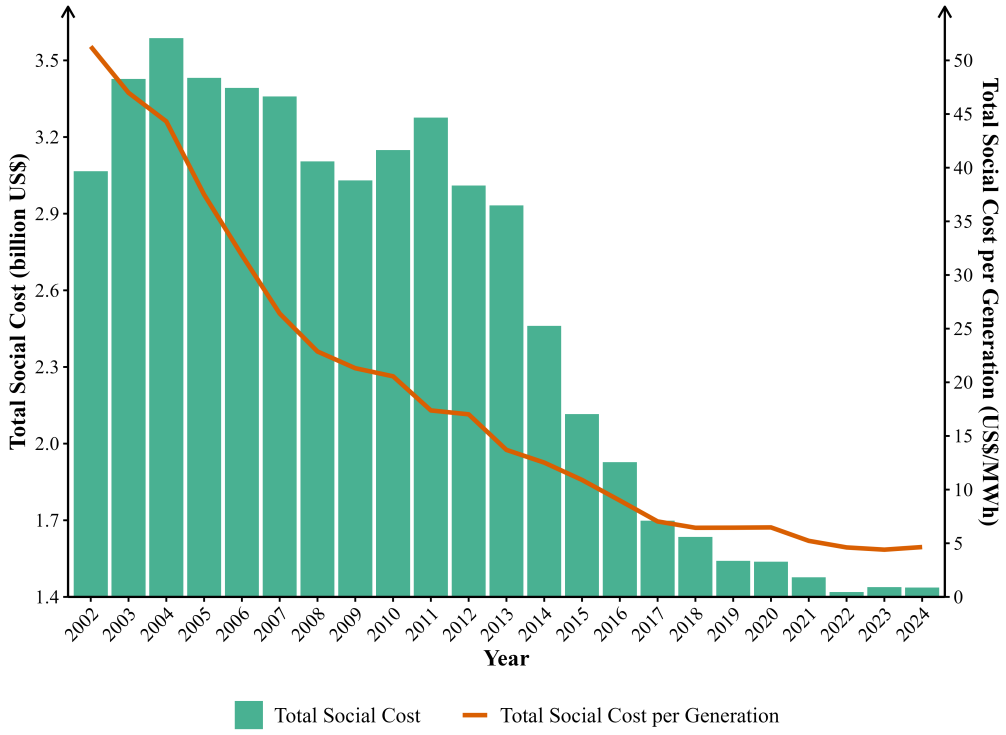


Figure 16: Social costs saved from gas-for-coal substitution strategy (2002–2024). The bar represents total cost savings (USD billion), and the line shows savings per unit of generation (USD/MWh).

Figure 16 shows the historical evolution of savings from such a substitution for China. Results indicate that gas-for-coal substitution could reduce China's social costs by USD 1.44 billion, equivalent to 33.70% of total losses under extreme heat. On average, this equals USD 4.65 per MWh, narrowing 5.92%–7.81% of the comprehensive generation cost gap between gas and coal.

Expanding the analysis to an international scale, benefits are highly concentrated in major coal-dependent, heat-prone economies. Figure 17 shows that when expressed in avoided mortality, India alone accounts for about 16,832 lives saved each year (84.22% of the global total), reflecting its high exposure to extreme heat, heavy coal reliance, and limited gas penetration. China ranks second, with roughly 1154 avoided deaths (5.78%). Together, the top ten countries capture more than 96% of global mortality benefits.

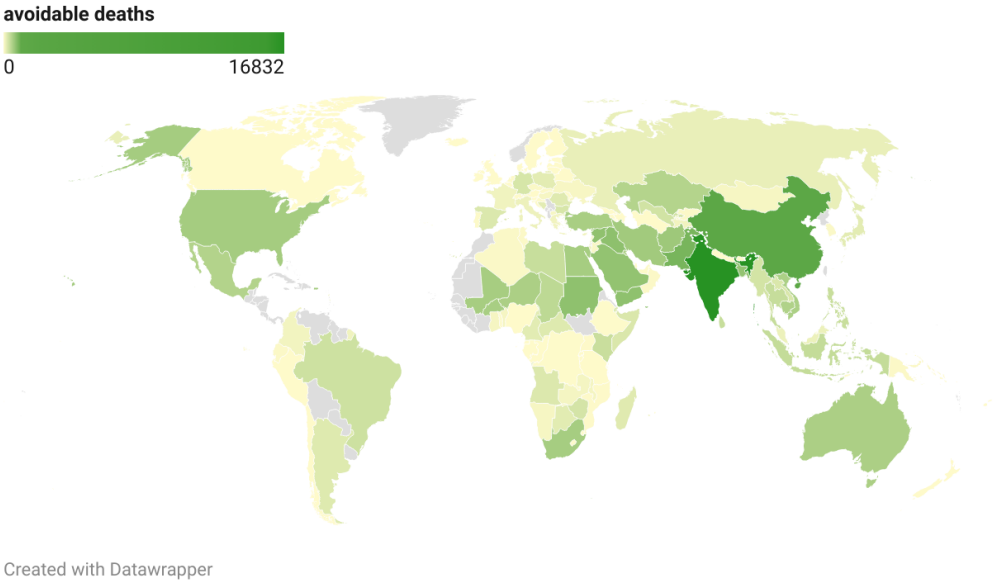


Figure 17: Avoided premature deaths under a full coal-to-gas substitution scenario.

The monetized welfare gains follow a similar geographic concentration (Figure D.6). India would save USD 20.06 billion annually, accounting for over 80% of the global total. For many smaller economies, absolute savings remain modest, but relative to GDP they represent substantial welfare improvements, reinforcing the case for targeted international support to accelerate clean fuel transitions in vulnerable regions. More discussions on gas-for -coal substitution are provided in Appendix D.

6 Discussion and Conclusions

Extreme heatwaves are becoming more frequent and intense under climate change, posing compound risks to energy systems, air quality, and public health. While prior studies have documented the co-occurrence of heat extremes and elevated pollution levels, most have focused on atmospheric chemistry, exposure pathways, or demand-side effects. Much less is known about

how heat stress directly impairs the operational efficiency of fossil-fuel power plants, thereby amplifying emissions, and how large the resulting health and economic damages might be.

This study provides the first causal evidence that extreme heatwaves elevate air pollution through the thermal-efficiency channel in real-world power plant operations. Using high-frequency operational, meteorological, and emissions data from Guangdong Province, we document that $PM_{2.5}$ emission intensity rises by 21.4% during extreme heat events, with coal-fired units exhibiting an additional 12.3% increase relative to gas-fired plants. These effects extend to other combustion-related pollutants, underscoring the robustness of the efficiency mechanism.

Welfare analysis indicates that the heatwave-induced efficiency losses currently account for about 3,981 premature deaths and USD 4.21 billion in annual social costs in China. The burden is not evenly distributed: industrial and coal-dependent provinces such as Zhejiang, Henan, Jiangsu, and Guangdong experience the sharpest efficiency-induced pollution increases, while hydropower-rich provinces like Yunnan and Sichuan show more muted responses. Looking ahead, under the high-emissions SSP5–8.5 scenario, projected to produce about 4.4° of warming by 2100, China's annual costs could escalate nearly fivefold to USD 20.41 billion, with disproportionate impacts falling on already vulnerable provinces.

At the global scale, these dynamics translate into approximately 76.21 billion USD in annual social costs, with India and China together accounting for nearly 80% of premature deaths and more than two-thirds of total damages. Our counterfactual analysis shows that replacing coal-fired generation with gas-fired alternatives could substantially mitigate heatwave-related damages, particularly in large, coal-dependent economies.

These findings carry three broad implications. First, they underscore the societal risks of continued coal dependence and the urgency of advancing climate-resilient, low-carbon energy transitions in a warming world. Second, diversifying generation portfolios away from coal offers a "double dividend," cutting baseline emissions while reducing their amplification during extreme heat events. Third, power sector regulation and market design need to reflect temperature-sensitive damages in dispatch, capacity planning, and investment. Existing emissions pricing mechanisms typically assume static marginal damages, overlooking the climate-driven variability revealed here.

Several limitations should be noted. We identify five plausible mechanisms for efficiency loss, including reduced cooling capacity, degraded combustion efficiency, and pollution control inefficiencies. However, we cannot directly quantify their individual contributions due to data constraints. Our empirical analysis focuses on a single province and event; while Guangdong's scale and energy mix make it broadly representative of other industrialized regions in developing economies, broader validation across multiple countries and events is needed. Global extrapolations also rely on projected heatwave frequencies and generation mixes, which may not fully reflect local adaptation measures or technology upgrades.

Acknowledgements

We gratefully acknowledge financial support from the National Key Research and Development Program of China (Grant No. 2024YFF0809202 for Q.C., Y.W., and C.W.), the National Natural Science Foundation of China (Grant No. 72203218 for B.G. and Grant No. 72503244 for P.S.), the Fundamental Research Funds for the Central Universities, and the Research Funds of Renmin University of China (Grant No. 25XNN063 for B.G. and No. 24XNF059 for P.S.).

References

Burnett, R., Chen, H., Szyszkowicz, M., Fann, N., Hubbell, B., Pope III, C. A., Apte, J. S., Brauer, M., Cohen, A., Weichenthal, S., et al. (2018). Global estimates of mortality associated with long-term exposure to outdoor fine particulate matter. *Proceedings of the National Academy of Sciences*, 115(38):9592–9597.

Chang, T., Graff Zivin, J., Gross, T., and Neidell, M. (2016). Particulate pollution and the productivity of pear packers. *American Economic Journal: Economic Policy*, 8(3):141–169.

Chang, T. Y., Graff Zivin, J., Gross, T., and Neidell, M. (2019). The effect of pollution on worker productivity: evidence from call center workers in china. *American Economic Journal: Applied Economics*, 11(1):151–172.

Cheng, C., Liu, Y., Han, C., Fang, Q., Cui, F., and Li, X. (2024). Effects of extreme temperature events on deaths and its interaction with air pollution. *Science of the Total Environment*, 915:170212.

Cohen, A. J., Brauer, M., Burnett, R., Anderson, H. R., Frostad, J., Estep, K., Balakrishnan, K., Brunekreef, B., Dandona, L., Dandona, R., et al. (2017). Estimates and 25-year trends of the global burden of disease attributable to ambient air pollution: an analysis of data from the global burden of diseases study 2015. *The Lancet*, 389(10082):1907–1918.

Fu, S., Viard, V. B., and Zhang, P. (2021). Air pollution and manufacturing firm productivity: Nationwide estimates for china. *The Economic Journal*, 131(640):3241–3273.

Gao, M., Wang, F., Xu, Y., Chen, J., Lu, X., and Carmichael, G. R. (2024). Future intensification of co-occurrences of heat, pm2. 5 and o3 extremes in china and india despite stringent air pollution controls. *Environmental Research Letters*, 20(1):014044.

Geng, G., Liu, Y., Liu, Y., Liu, S., Cheng, J., Yan, L., Wu, N., Hu, H., Tong, D., Zheng, B., et al. (2024). Efficacy of china's clean air actions to tackle pm2. 5 pollution between 2013 and 2020. *Nature Geoscience*, 17(10):987–994.

Giguere, J., Otto, F. E. L., Tannenbaum, A., Vahlberg, M., et al. (2025). Climate change and the escalation of global extreme heat: Assessing and addressing the risks. Heat Action Day 2025 Report.

Grant, L., Vanderkelen, I., Gudmundsson, L., Fischer, E., Seneviratne, S. I., and Thiery, W. (2025). Global emergence of unprecedented lifetime exposure to climate extremes. *Nature*, 641(8062):374–379.

Greenstone, M., Pande, R., Ryan, N., and Sudarshan, A. (2025). Can pollution markets work in developing countries? experimental evidence from india. *The Quarterly Journal of Economics*, 140(2):1003–1060.

He, J., Liu, H., and Salvo, A. (2019). Severe air pollution and labor productivity: Evidence from industrial towns in china. *American Economic Journal: Applied Economics*, 11(1):173–201.

IEA (2025). Global energy review 2025. Licence: CC BY 4.0.

IPCC (2023). *Climate Change 2023: Synthesis Report. Contribution of Working Groups I, II and III to the Sixth Assessment Report of the Intergovernmental Panel on Climate Change*. Intergovernmental Panel on Climate Change, Geneva, Switzerland. Core Writing Team.

Jiang, L., Yang, Y., Wu, Q., Yang, L., and Yang, Z. (2024). Hotter days, dirtier air: the impact of extreme heat on energy and pollution intensity in china. *Energy Economics*, 130:107291.

Liu, S., Shu, L., Zhu, L., Song, Y., Sun, W., Chen, Y., Wang, D., Pu, D., Li, X., Sun, S., et al. (2024). Underappreciated emission spikes from power plants during heatwaves observed from space: Case studies in india and china. *Earth's Future*, 12(2):e2023EF003937.

Muller, N. Z. and Mendelsohn, R. (2007). Measuring the damages of air pollution in the united states. *Journal of Environmental Economics and Management*, 54(1):1–14.

Orellano, P., Reynoso, J., and Quaranta, N. (2021). Short-term exposure to sulphur dioxide (so2) and all-cause and respiratory mortality: A systematic review and meta-analysis. *Environment International*, 150:106434.

Pope Iii, C. A., Burnett, R. T., Thun, M. J., Calle, E. E., Krewski, D., Ito, K., and Thurston, G. D. (2002). Lung cancer, cardiopulmonary mortality, and long-term exposure to fine particulate air pollution. *JAMA*, 287(9):1132–1141.

Rahman, M. M., McConnell, R., Schlaerth, H., Ko, J., Silva, S., Lurmann, F. W., Palinkas, L., Johnston, J., Hurlburt, M., Yin, H., et al. (2022). The effects of coexposure to extremes of heat and particulate air pollution on mortality in california: implications for climate change. *American Journal of Respiratory and Critical Care Medicine*, 206(9):1117–1127.

Schnell, J. L. and Prather, M. J. (2017). Co-occurrence of extremes in surface ozone, particulate matter, and temperature over eastern north america. *Proceedings of the National Academy of Sciences*, 114(11):2854–2859.

Shen, J., Zhang, S., Zhao, M., Zhang, C., Cai, W., and Wang, C. (2025). Improving cost–benefit analyses for health-considered climate mitigation policymaking. *Nature Climate Change*, pages 1–10.

Somanathan, E., Somanathan, R., Sudarshan, A., and Tewari, M. (2021). The impact of temperature on productivity and labor supply: Evidence from indian manufacturing. *Journal of Political Economy*, 129(6):1797–1827.

Wang, Y., Wang, Q., Ye, J., Li, L., Zhou, J., Ran, W., Zhang, R., Wu, Y., and Cao, J. (2020). Chemical composition and sources of submicron aerosols in winter at a regional site in beijing-tianjin-hebei region: Implications for the joint action plan. *Science of the Total Environment*, 719:137547.

World Bank (2022). *Electricity production from coal sources (% of total)*. World Development Indicators, The World Bank Group.

World Bank and IHME (2016). *The Cost of Air Pollution: Strengthening the Economic Case for Action*. World Bank, Washington, DC.

Xie, T., Yuan, Y., and Zhang, H. (2023). Information, awareness, and mental health: Evidence from air pollution disclosure in china. *Journal of Environmental Economics and Management*, 120:102827.

Xu, R., Huang, S., Shi, C., Wang, R., Liu, T., Li, Y., Zheng, Y., Lv, Z., Wei, J., Sun, H., et al. (2023). Extreme temperature events, fine particulate matter, and myocardial infarction mortality. *Circulation*, 148(4):312–323.

Yang, J. and Shao, M. (2021). Impacts of extreme air pollution meteorology on air quality in china. *Journal of Geophysical Research: Atmospheres*, 126(7):e2020JD033210.

Zhang, X., Zhang, X., and Chen, X. (2017). Happiness in the air: How does a dirty sky affect mental health and subjective well-being? *Journal of Environmental Economics and Management*, 85:81–94.

Zhong, Q., Shen, G., Wang, B., Ma, J., and Tao, S. (2025). Climate-driven escalation of global pm2. 5 health burden from wildland fires. *Environmental Science & Technology*.

Zivin, J. G. and Neidell, M. (2012). The impact of pollution on worker productivity. *American Economic Review*, 102(7):3652–3673.

Appendices

A Other social cost estimates

To test the robustness of our main results, we apply two alternative approaches for estimating the social costs of heatwave-induced efficiency losses in fossil-fuel power plants in China.

First, we calculate social costs using province-level parameters rather than national averages. Specifically, the estimation incorporates heterogeneity in pollutant concentrations, generation mix, and the share of power plant emissions in each province's total emissions. Provincial social costs are then aggregated to obtain the national total. The results are consistent with national-level estimates, confirming the reliability of the country-level data used in the main text.

Second, we implement a Pollution Expansion Range Approach. In this approach, we define a radius of 10 km around each fossil-fuel power plant, within which efficiency losses during extreme heatwaves are assumed to measurably affect local air quality. Population exposure is then restricted to residents within these areas. Using the same valuation framework as in the main text, we calculate plant-level social costs and sum them to obtain national totals. For this calculation, we use data on all 1,112 thermal power generation units in China from the Global Energy Observatory, along with 2022 LandScan Global Population Database data to determine the population within each plant's 10 km radius. This method yields an estimate of USD 3.59 billion, which is close to the USD 4.21 billion from the province-level approach and the USD 3.53 billion from the national aggregate method.

Table A.1: Comparison of social cost estimates using multiple methods

	Total Social Cost (million USD)	Total Population Covered (millions)
China-as-a-whole	3528.8	1220.87
Province-level	4210.4	1419.50
10 km radius	3591.7	940.57

Table A.1 compares the results across these methods. The close alignment among them demonstrates the robustness of our estimates for China's social costs under extreme heatwave conditions.

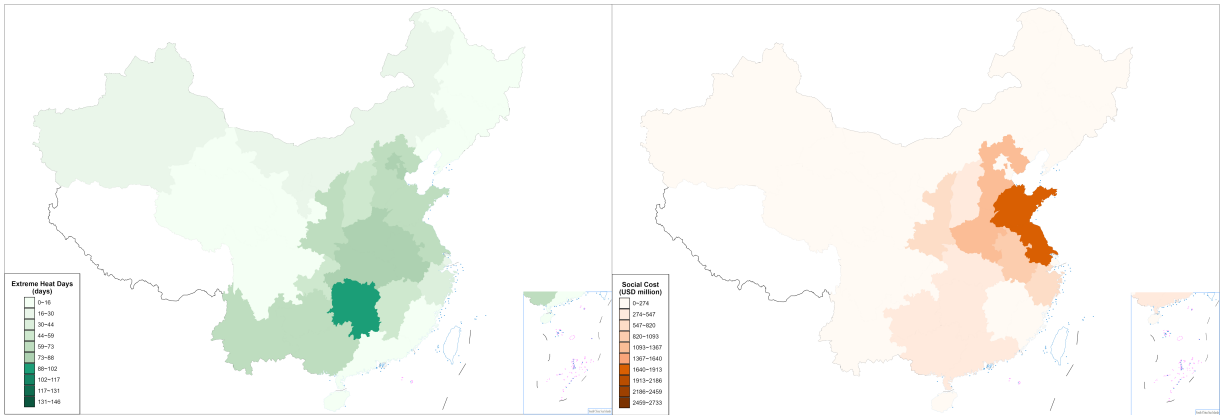
B China's social costs under different SSP scenarios

We also evaluate two alternative emissions scenarios: a medium-emissions pathway (SSP2–4.5) and a low-emissions pathway (SSP1–2.6). As shown in Table B.2, annual premature deaths attributable to heatwave-induced efficiency losses could rise to 11,817 under SSP2–4.5 and 11,693 under SSP1–2.6, corresponding to social costs of USD 12.50 billion and USD 12.37 billion—about three times the present-day estimate. Figure B.1 provides detailed provincial

results, including the number of hot days (Figure B.1a) and associated social costs (Figure B.1b) under SSP2–4.5, as well as projections for hot days (Figure B.2a) and social costs (Figure B.2b) under SSP1–2.6. Even under more ambitious mitigation scenarios, projected annual social costs remain above USD 12 billion, underscoring the persistence of climate-related efficiency risks and their societal impacts in a warming world.

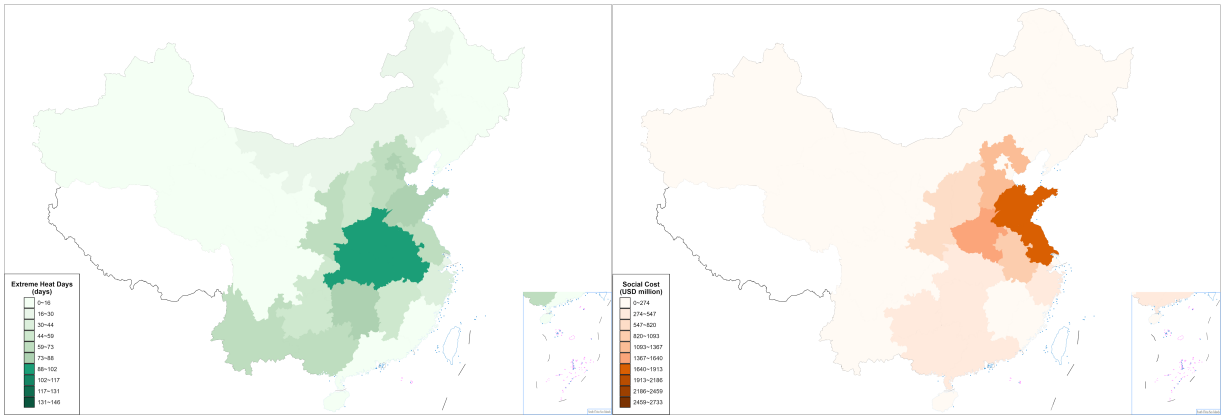
Table B.2: Projected Premature Deaths and Social Costs in China under Alternative Climate Scenarios.

RCP Scenario	Extreme heat days	Premature deaths	Social cost (USD billion)
Low emissions (SSP1-2.6)	50.4	11,693	12.37
Medium emissions (SSP2-4.5)	51.0	11,817	12.50
High emissions (SSP5-8.5)	83.7	19,292	20.41



(a) Projected number of hot days in each province (b) Estimated social costs across provinces

Figure B.1: Projected provincial outcomes under the SSP2–4.5 medium-emissions scenario.



(a) Projected number of hot days in each province (b) Estimated social costs across provinces

Figure B.2: Projected provincial outcomes under the SSP1–2.6 low-emissions scenario.

C Country-specific VSL estimates

In the main text, we quantified premature mortality and social costs from heat-induced efficiency losses using a uniform global VSL of USD 1.19 million, ensuring cross-country comparability. Here, we extend the analysis by applying country-specific VSLs, derived from per capita GDP, to capture income heterogeneity in damage valuation.

Globally, this approach yields an estimated annual social cost of USD 21.90 billion, far lower than the USD 76.21 billion obtained under the uniform VSL assumption. The downward shift is largely explained by India: while it accounts for the majority of premature deaths, its VSL is only about USD 0.14 million—substantially below the global reference value. Similar effects apply to other populous developing economies with low income-adjusted VSLs.

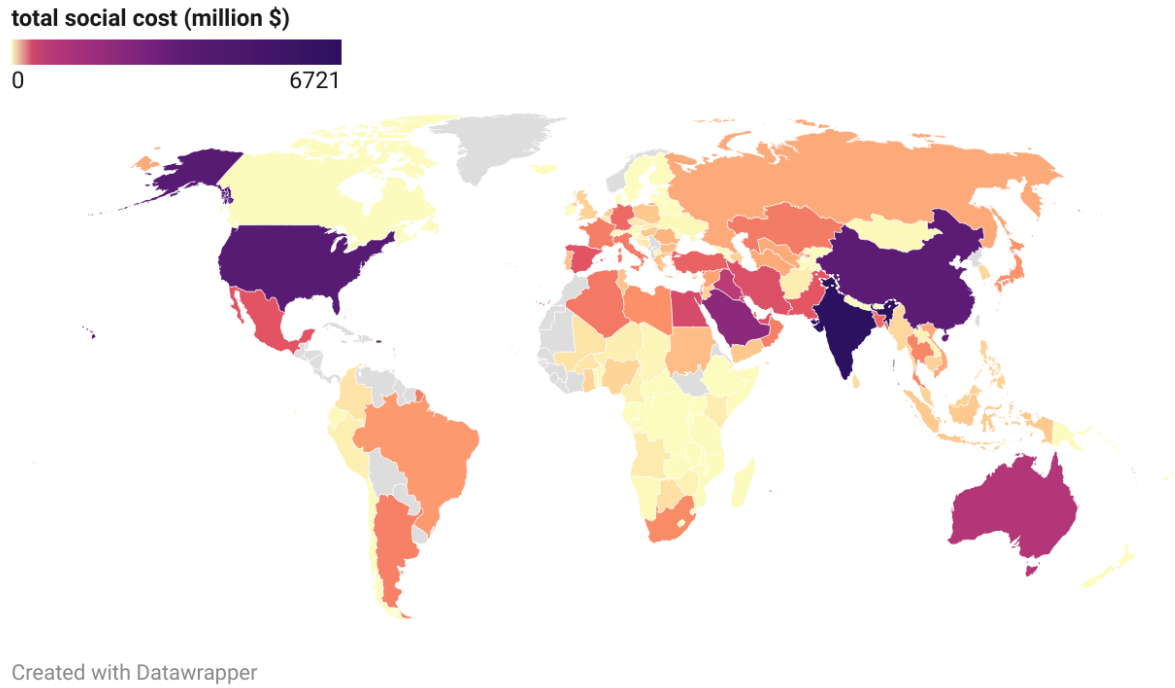


Figure C.3: Global distribution of social costs (million USD) under country-specific VSL estimates. Darker shading indicates higher total social costs, with the largest burdens concentrated in India, China, the United States, and selected Middle Eastern economies.

Figure C.3 maps the global distribution of estimated social costs. The spatial pattern highlights pronounced disparities: India and China remain dominant contributors in absolute terms, yet their relative shares diminish compared with the uniform VSL assumption due to lower income levels. By contrast, high-income economies such as the United States and Australia register larger shares of global costs despite comparatively fewer premature deaths. Oil-exporting economies in the Middle East—including Saudi Arabia, Kuwait, and the United Arab Emirates—also feature prominently given their higher income-adjusted VSLs. These results illustrate how reliance on income-based valuation metrics can reshape perceptions of global pollution damages and accentuate inequities in the distribution of climate-related welfare losses.

The top ten contributors to global social costs—India, the United States, China, Saudi Ara-

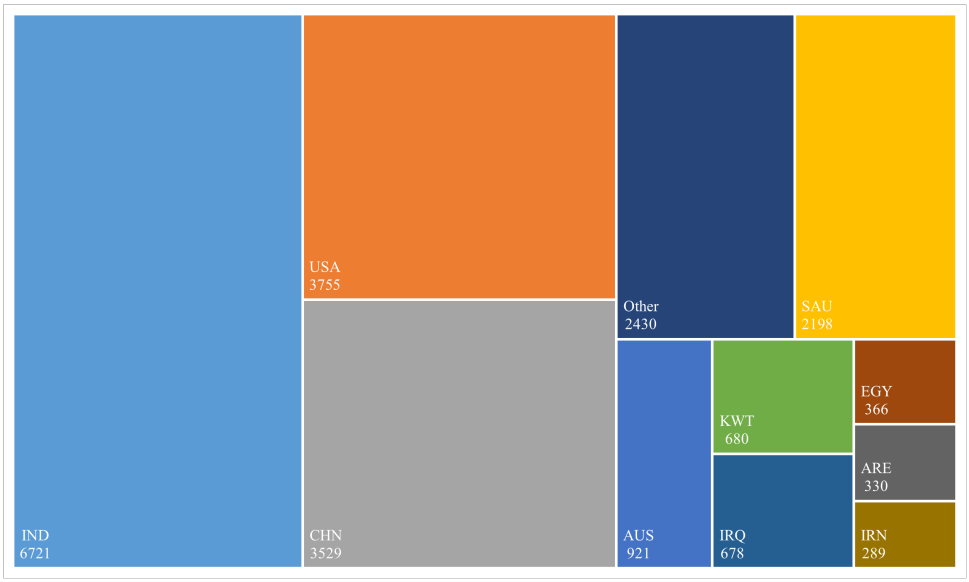


Figure C.4: Global social costs under heterogeneous country-specific VSLs (top 10 countries in million USD). Estimates show substantial differences compared with uniform VSL assumptions, reflecting cross-country income disparities.

bia, Australia, Kuwait, Iraq, Egypt, the United Arab Emirates, and Iran—together account for 88.90% of the total (Figure C.4). Notably, the overlap with the top-ten list for premature deaths is only partial: six countries (China, India, Saudi Arabia, Iraq, Egypt, and Iran) appear in both rankings but with markedly different positions. These divergences underscore the influence of income heterogeneity: for example, the United States contributes just 0.63% of global premature deaths but 17.15% of global social costs, whereas India represents 74.90% of deaths but only 30.69% of costs. Such differences highlight the distributional consequences of using heterogeneous VSLs and underscore the need for equity-sensitive approaches in global climate policy assessments.

D Gas-for-coal substitution

Figure D.5 decomposes the historical savings from gas-for-coal substitution for China by pollutant. NO_3^- dominates the savings, with its share rising steadily to 81.80% in 2024. By contrast, contributions from $PM_{2.5}$ and SO_4^{2-} exposures have declined to 12.51% and 5.69%, respectively. This shift largely mirrors the overall structure of social costs, underscoring the persistence of nitrate-related damages as the main driver.

Figure D.6 presents the monetized welfare gains from a global gas-for-coal substitution. India would save USD 20.06 billion annually—over 80% of the global total. For many smaller economies, absolute savings remain modest, but relative to GDP they represent substantial welfare improvements, reinforcing the case for targeted international support to accelerate clean fuel transitions in vulnerable regions.

Figure D.7 compares pollutant-specific savings across the top ten countries whose power system are the most fragile to extreme heatwaves. Patterns vary considerably depending on

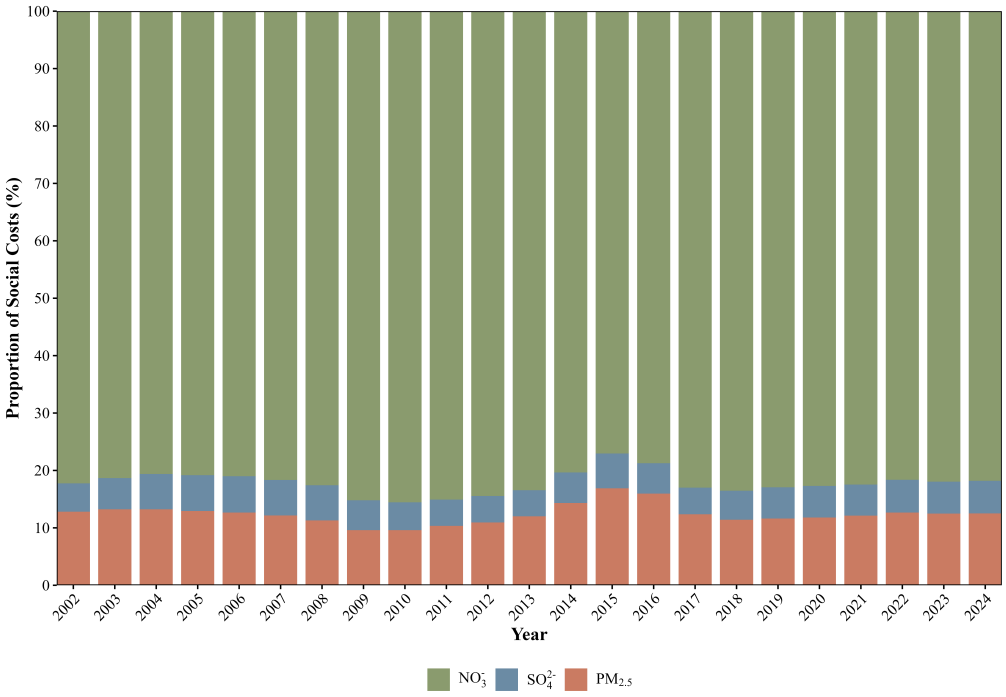


Figure D.5: Decomposition of social cost savings by pollutant type under the gas-for-coal substitution strategy (2002–2024)

national generation mixes and coal reliance. Heavily coal-dependent economies record larger reductions in NO_3^--related costs, whereas in others, $PM_{2.5}$ or SO_4^{2-} play a more prominent role. These differences highlight how baseline conditions and transition pathways shape the pollutant-level benefits of fuel switching.

Finally, Figure D.8 reports results under country-specific VSLs. Clear contrasts emerge: in the United States, relatively modest mortality reductions translate into large monetary benefits due to its high VSL, with savings concentrated in NO_3^- exposure reductions. In contrast, India achieves the largest mortality reduction but far smaller monetized benefits, reflecting its low income-adjusted VSL and more balanced pollutant profile. These comparisons illustrate how both valuation frameworks and baseline conditions influence the distribution of benefits from gas-for-coal substitution.

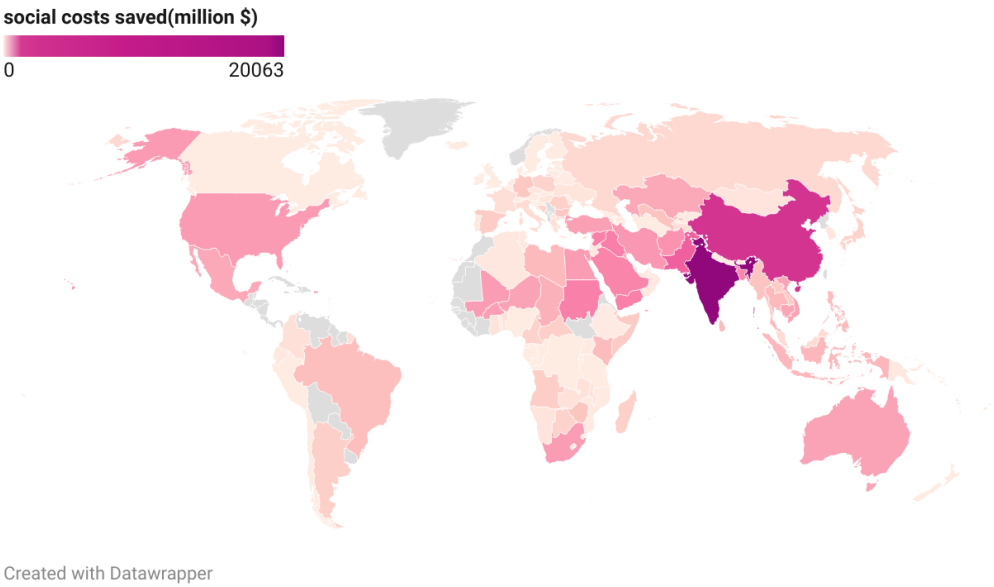


Figure D.6: Avoided social costs under a full coal-to-gas substitution scenario

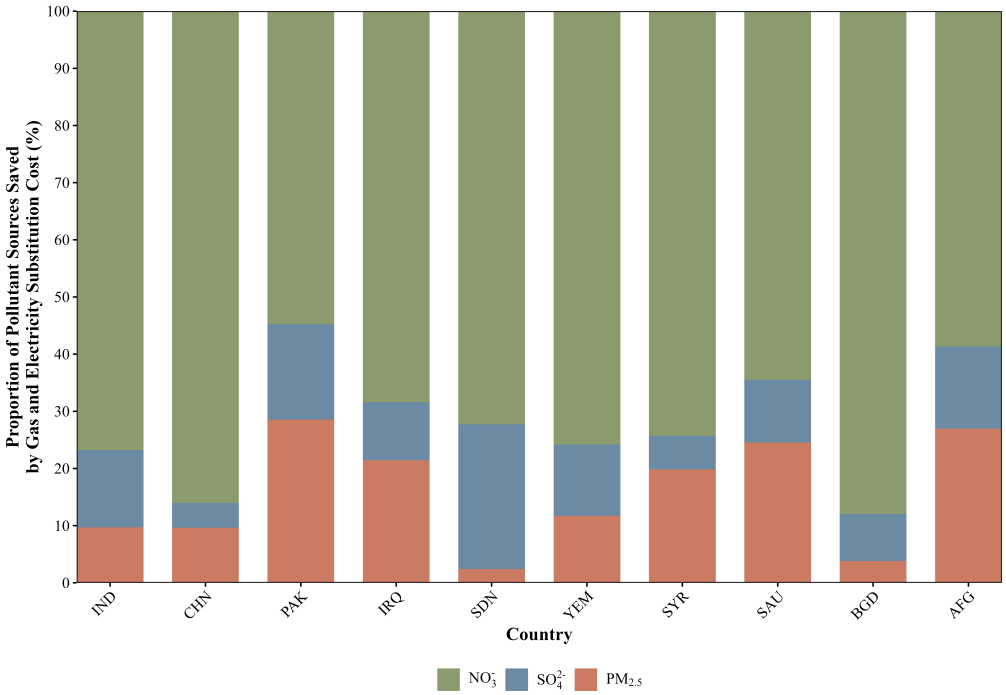


Figure D.7: Pollutant contribution to social cost savings from the gas-for-coal substitution strategy (top ten countries)

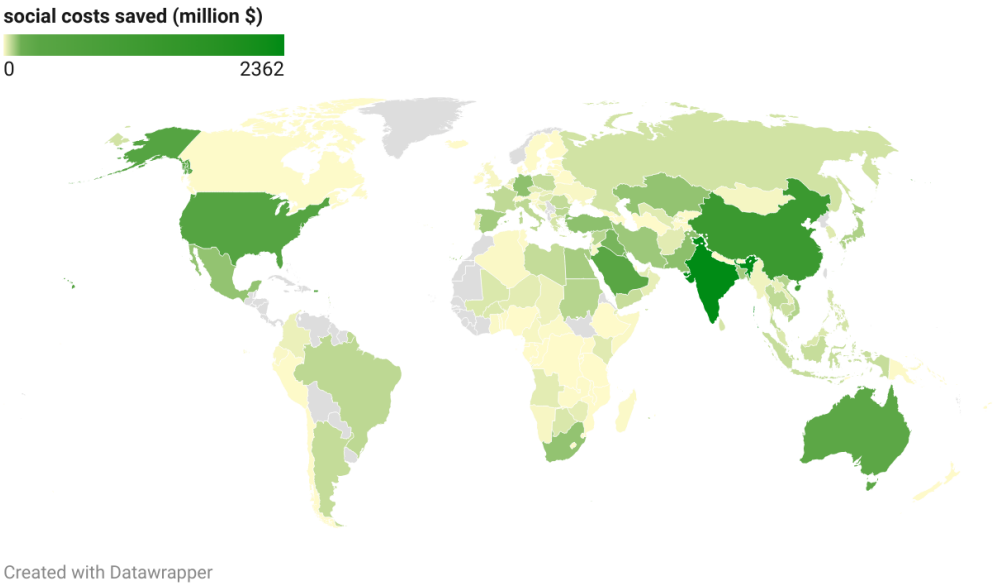


Figure D.8: Global social cost savings from the gas-for-coal substitution strategy under country-specific VSLs